Stony Brook University

The Influence of Proton Order on the Thermal Conductivity of Ice

A Thesis presented

by

Jonathan Tammo Siebert

to

The Graduate School

in Partial Fulfillment of the

Requirements

for the Degree of

Master of Arts

in

Physics

Stony Brook University

August 2014

Stony Brook University

The Graduate School

Jonathan Tammo Siebert

We, the thesis committee for the above candidate for the

Master of Arts degree, hereby recommend

acceptance of this thesis

Maria V. Fernandez-Serra - Thesis Advisor
Professor - Department of Physics and Astronomy

Matthew Dawber
Professor - Department of Physics and Astronomy

Philip B. Allen
Professor - Department of Physics and Astronomy

Joanna Kiryluk
Professor - Department of Physics and Astronomy

This thesis is accepted by the Graduate School

Charles Taber
Dean of the Graduate School

Abstract of the Thesis

The Influence of Proton Order on the Thermal Conductivity of Ice

by

Jonathan Tammo Siebert

Master of Arts

in

Physics

Stony Brook University

2014

Water is one of the most important reasons for the possibility of life on earth. Even though water and ice have been in the focus of countless studies they are far from being understood. Despite their simple molecular structure, especially the ability of the molecule to form hydrogen bonds leads to a variety of interesting properties. One of them is the density maximum of water in its liquid state. This is caused by the hydrogen bound hexagonal structure of low pressure ice.

In this work the influence of proton ordering on the thermal conductivity of hexagonal ice is examined. It is experimentally impossible to achieve a pure sample of proton ordered hexagonal ice because of the frozen proton mobility at low temperatures. Therefore, in this work, proton ordered and unordered ice is studied using non-equilibrium molecular dynamics simulations.

Proton ordered and unordered cells are simulated at different temperatures. The used empirical force field model is shown to reproduce the experimentally expected increase of the thermal conductivity for the ordered cells. Also the increase of thermal conductivity for lower temperatures is reproduced qualitatively.

Contents

List of Figures

List of Tables

Acknowledgment

I want to thank everyone whose support allowed me to study. Explicitly I want to thank the following people and organizations whose backing allowed me to write this thesis.

- Most importantly, I want to thank Professor Marivi Fernandez-Serra for her excellent supervision. She provided me with this interesting topic and always supported me with helpful comments, assistance and encouragement. Also she provided me with several scripts and programs that have been used in this work.
- I am also very grateful to Professor Philip B. Allen for the very helpful discussions and comments concerning my work.
- Furthermore, I want to thank Professor Philip B. Allen, Professor Matthew Dawber and Professor Joanna Kiryluk for serving on my thesis defense committee.
- The Fulbright program is gratefully acknowledged for nine months of financial support, allowing me to study at this university.
- Also I want to thank my parents, Albert Schneider and Kathrin Siebert, for their ongoing emotional and financial support during all of my studies, as well as for pointing out several spelling mistakes in this work.
- Last, I want to thank my girlfriend, Janine Tappe, for her incredible emotional support and also the proofreading of this work.

1 Introduction

Water is one of the most important, if not the most important, reasons for the possibility of life on earth. It covers over 70% of the earth's surface and gave our "blue planet" its name. Without water life on earth as we know it would be impossible.

Despite its rather simple molecular structure of two hydrogen atoms being bound to one oxygen atom, it shows a variety of interesting properties. One of the reasons for this is the large dipole moment of the molecule arising from the big difference in electronegativity between oxygen and hydrogen. This allows the molecule to form hydrogen bonds. These bonds are responsible for example for the structure of ice at low pressure which causes ice to float on liquid water due to its smaller density. This is the best known of the several anomalous properties of water.

Because of its importance and its many interesting properties, many studies have examined water in its many solid, liquid and gaseous phases. Whole books have been published just about the up to now 15 crystal and two amorphous as well as the meta-stable known solid phases. A detailed discussion of many properties of ice is for example given in the book by Petrenko and Whitworth [23].

Although it has been under investigations for a very long time, water in general and ice in particular are still far from understood. The physics of water and ice is still a very active area of research.

In recent years computer simulations have been established as an additional method apart from experimental and theoretical research. It allows to test experimental setups before they are built or to test theoretical predictions before they can be validated in expensive experiments. In comparing them with the theoretical and experimental results, the simulation methods can be refined and this leads to a further improvement of the available simulation methods.

But simulations do not only play a supplementary role. They allow to examine systems in a very controlled way. The effects of interest can be probed in an isolated way without the constraints of an experiment. Also experimentally not achievable configurations can be explored. The proton ordered phase of ice, ice XI, that is examined in this work, is stable under 72K, but because of the low proton mobility, it is impossible to produce a pure sample. In the simulations, on the other hand, the protons can be set arbitrarily. Even proton-ordered ice at temperatures much higher than the

transition temperature can be measured.

In this work, the influence of the proton ordering on the thermal conductivity is examined by use of the direct method proposed by Müller-Plathe [20]. Similar studies have already been done for liquid water, for example by Bedrov and Smith [6], by Bresme [8], by Zhang, Lussetti, de Souza, and Müller-Plathe [34] and a very recent study doing a very thorough examination of multiple temperatures and pressures by Römer, Lervik, and Bresme [26]. A study of proton disordered ice using an equilibrium method has been done by English, Tse, and Gallagher [11].

Experimentally, the influence of the proton ordering on the thermal conductivity has been measured in KOH doped, partially proton-ordered ice. This was done for example by Andersson and Suga [4]. In this work now the thermal conductivity of fully proton-ordered pure ice as well as of proton-unordered ice is studied by simulations and compared. This will allow to check whether the flexibility of the used TIP4P/2005f model introduces a sufficient coupling between the intra- and inter-molecular bonds to capture the differences in the hydrogen bond's strengths for different proton configurations. This is mandatory to reproduce the difference in thermal conductivity between the proton-ordered and unordered case.

In section 2 a definition and explanation of the thermal conductivity as well as some properties of water and the used water model are given. In section 3 the used simulation and evaluation methods are explained. Afterwards section 4 presents the results obtained by this work. In the last section 5 a short summary and suggestions for future work on this topic are given.

2 Background

The goal of this work is to examine the thermal conductivity of ice under different conditions. This chapter gives a short overview over the theoretical background. The thermal conductivity will be introduced and some properties of water and ice will be listed.

2.1 Thermal Conductivity

The thermal conductivity characterizes the ability of a material to transport heat. Fourier's law is the empirical relation between a heat current $\vec{J}$ and a thermal gradient defining the thermal conductivity κ_{ij} as:

$$J_i = -\sum_j \kappa_{ij} \partial_j T. \tag{1}$$

It is only valid in a linear response regime, where the temperature gradient is not too extreme. The minus sign accounts for the fact, that the heat will always flow from hot to cold and therefore against the thermal gradient. In an approximately isotropic and homogeneous material the thermal conductivity reduces to a positive scalar:

$$\vec{J} = -\kappa \cdot \nabla T. \tag{2}$$

The thermal conductivity is not a constant material property but it is strongly temperature dependent. The absolute form of the temperature dependence is determined by the type of the dominant heat carriers. In an insulator such as ice the main heat carriers are phonons. The finiteness of κ mainly arises from scattering of phonons in three phonon anharmonic scattering, scattering of defects and scattering of the boundary of the crystal.

In the Debye model an estimate of thermal conductivity can be easily derived. The full derivation can be found for example in Ashcroft and Mermin [5, p. 495ff]. Their derivation uses kinetic theory as follows.

Let $\epsilon(T)$ be the energy density of the crystal at temperature T. In the relaxation time approximation the phonon scattering events are treated in an averaged way. These events are considered to take place on average after a time interval τ. After each scattering, the phonon will move in a random direction. Since the derivation follows the Debye model, the velocity of the phonon is taken to be the sound velocity c of the crystal. The mean free

path $l = c\tau$ is assumed constant. Therefore, the heat flow given at point $\vec{x}_0 = (x, y, z_0)^{\mathrm{T}}$ can be computed by averaging over the energies of those phonons, that scattered last on a sphere around $\vec{x}_0$ with radius l:

$$\vec{J} = \langle \vec{c} \cdot \epsilon(T) \rangle_{\text{sphere}}. \tag{3}$$

Due to the symmetry the x and y components become zero. For the heat current in the z direction one gets:

$$\begin{aligned} J_z &= \langle c_z \cdot \epsilon\left(T(z)\right) \rangle_{\text{sphere}} \\ &= \frac{1}{4\pi} \int_{-1}^{1} \mathrm{d}\cos(\theta) \int_0^{2\pi} \mathrm{d}\phi \ \mathrm{c_z} \cdot \epsilon\left(\mathrm{T(z)}\right) \\ &\approx \frac{1}{2} \int_{-1}^{1} \mathrm{d}\cos(\theta) \ \mathrm{c}\cos(\theta) \left(\epsilon(\mathrm{T(z_0)}) + \partial_{\mathrm{z}} \epsilon(\mathrm{T(z_0)}) \cdot (\mathrm{z} - \mathrm{z_0})\right) \\ &= -\frac{1}{3} c l \partial_T \epsilon(T(z_0)) \partial_z T(z_0), \end{aligned} \tag{4}$$

where after the second step the energy was expanded linearly in z and in the third step, $z - z_0$ was set to $l\cos(\theta)$. So the thermal conductivity in this approximation is given by:

$$\kappa = \frac{1}{3} c_v c l, \tag{5}$$

where $c_v = \partial_T \ \epsilon(T)$ is the specific heat of the crystal.

Apparently the thermal conductivity is proportional to the mean free path of the phonons in the crystal. As mentioned earlier, there are several competing processes with different mean free paths l_i. In the case of competing scattering effects the effective mean free path l_{eff} is given in good approximation by Matthiessen's rule:

$$\frac{1}{l_{\text{eff}}} = \sum_i \frac{1}{l_i}. \tag{6}$$

In an experimental setup of a pure crystal, the contributions of impurity and boundary scattering will be smaller than the contribution of three phonon scattering events. The temperature dependence of the thermal conductivity can be understood by examining the probability of phonon scattering events. This is also explained in [5, p. 501ff].

They argue that the temperature dependence in the high temperature regime is dominated by the temperature evolution of the mean phonon occupation numbers. The specific heat approaches the constant limit of the Dulong and Petit law for high temperatures. The sound velocity is also not strongly temperature dependent. But the mean phonon occupation number is approximately proportional to the temperature. The exact form of the thermal conductivity's temperature dependence is governed by the exact type of scattering dominant in the crystal. Even without knowledge of the phonon scattering probabilities they claim that the temperature dependence is usually given by a power law of type $\kappa \propto T^{-x}$, where x is between one and two.

Still following [5] one finds that the thermal conductivity in the low temperature regime is dominated by two competing effects. First by lowering the temperature far enough umklapp processes are frozen out in the crystal, because mostly phonons with small wave vectors are present. Normal processes do not change the total phonon wave vector and therefore do not allow the crystal to reach equilibrium. This leads to an exponential increase in thermal conductivity for very low temperatures. According to their explanation the phonon mean free path increases rapidly until it reaches the range where impurity and boundary scattering start to dominate. Then the temperature dependence will be dominated by the T^3 decrease of the specific heat for temperatures lower than the Dulong Petit regime.

The very large mean free path of phonons for low temperatures, and the importance of quantum effects in that regime, prevents this work's method from being used in determination of the thermal conductivity. Therefore, in this work only the high temperature limit will be examined.

2.2 Properties of Water and Ice

In this work ice is studied. Despite its rather simple molecular structure, H_2O shows a very interesting behavior. Due to its prevalence and its importance to life on earth it has been subject of many studies. Whole books have been published about its properties. The properties listed here are taken from Petrenko and Whitworth [23]. Their book gives a good overview over the properties of the solid phases of water.

Many of the interesting properties of water and ice arise from the polar structure of the molecule. Because of the high electronegativity of oxygen, most of the negative charge of the molecule is located around the oxygen

atom. This allows the molecules to form hydrogen bonds.

Hydrogen bonds are responsible for the most commonly known anomalous properties of water. Due to its structure the low pressure phase of ice has a lower density than liquid water. Therefore, ice is able to float on water. There are several other phases of water. The solid phases studied in this work are described in the next section.

2.2.1 Phases of Ice

By now 15 stable solid phases of water are known. The last phase, ice XV, was discovered in 2009 by Salzmann, Radaelli, Mayer, and Finney [27]. The phases differ in structure and are stable at different temperatures and pressures. At atmospheric pressure there are two stable and one metastable ice phase. The ice phase dominating in nature is ice Ih. Here the oxygen atoms are located in a hydrogen-bound hexagonal lattice. Every oxygen has four nearest neighbors. The hydrogen atoms are located along the hydrogen bonds obeying the ice rules found by Pauling [22]:[1]

1. Along each hydrogen bond one and only one hydrogen atom is located.

2. Each oxygen atom has exactly two hydrogen atoms covalently bound to it.

One possible structure is shown in figure 1a. Other than obeying these rules the hydrogen atoms are assumed to be distributed randomly across the crystal. This is only approximately correct. There are energy differences between the different configurations. Therefore, the configurations are not absolutely equally probable. For higher temperatures the energy differences are small enough to be discarded.

Because of the random distribution of hydrogen atoms, there is no long range order of the hydrogens. Therefore, this state is called proton disordered. The ice Ih phase is stable for pressures up to around 0.2GPa and above 72K. Between 130K and 220K there exists another metastable cubic phase called ice Ic, which is proton disordered as well.

For low temperatures the potential energy dominates the free energy. As stated in [23], for an energy gain of ΔE for occupying the lowest energy structure, the temperature must be smaller than $\Delta E/\Delta S_{\mathrm{hyd}}$. Here ΔS_{hyd} is

[1] Earlier an irregular structure had already been proposed by Bernal and Fowler [7].

the entropy resulting from the proton disorder. Its value is given at the end of this section. In this case the most stable structure will be the one with the lowest potential energy. It has been found by Tajima, Matsuo, and Suga [31] in 1984 that low pressure ice undergoes a phase transition to hexagonal ice XI at 72K. The resulting structure is proton ordered. Several structures have been suitable candidates for this structure. In 1985 Leadbetter, Ward, Clark, Tucker, Matsuo, and Suga [18] did a neutron diffraction experiment on KOD-doped heavy ice to find the structure of ice XI. Also in 2004 Hirsch and Ojamäe [14] did a quantum chemical calculation comparing the energy of all possible ordered orthorhombic structures with an eight molecule unit cell. They verified that the structure shown in figure 1b is the most stable.

Because of the low energy differences between the different hydrogen structures and the high energy barriers for a change in proton arrangement, the relaxation time for this first order phase transition is extremely long. Reordering of the protons requires reordering of multiple hydrogens at once for the ice rules to stay obeyed. Temporarily the ice rules have to be broken to allow reordering. So-called Bjerrum defects occur. If one hydrogen atom jumps to another bond it induces a D defect, which means two protons are located along one hydrogen bond and a L defect, meaning the lack of any proton along another hydrogen bond.

This transition is not observable on an experimental time scale. To shorten the relaxation time the crystal can be doped with alkali hydroxides. This method has also been used in the paper [31], which has been cited above. The doping introduces artificial Bjerrum defects, which allow relocation of the hydrogen bonds around the dopant in the crystal. After a long annealing time of up to 256h they found that one dopant ion allows approximately 15000 water molecules around it to rearrange into an ordered structure.

Because of the low proton mobility the transition is not observed in pure ice on an experimental timescale. Lowering the temperature below approximately 100K leads to a glass transition, where the proton positions are frozen. Haida, Matsuo, Suga, and Seki [13] did a calorimetric study showing the transition for pure ice. They cooled their sample quickly from 120K to temperatures between 89.4K and 107.6K. Afterwards they annealed their samples for a long time in a carefully isolated calorimetric chamber. They observed a temperature drift because of the proton ordering enthalpy relaxation. This verifies that partial ordering already occurs above the transition temperature. From the drift they estimated the relaxation time to increase

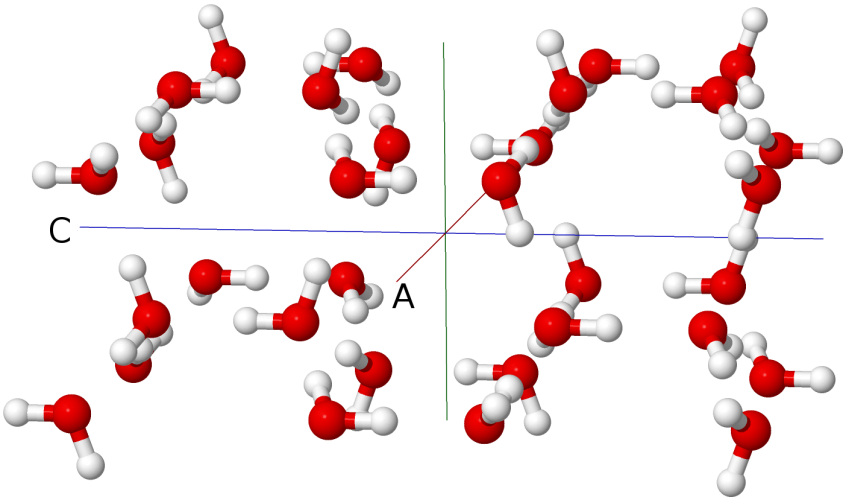

(a) Ice Ih

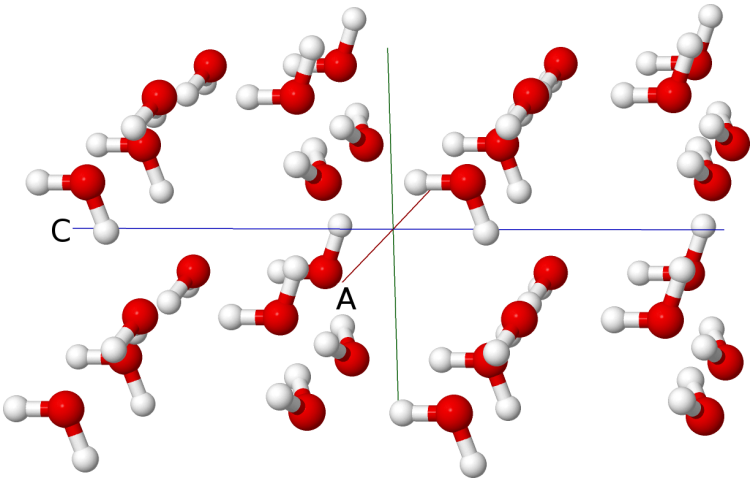

(b) Ice XI

Figure 1: The structure of ice Ih (a) and ice XI (b) are shown. Both pictures show 32 molecules. This corresponds to 8 unit cells of ice XI. Due to the proton-disorder in ice Ih there are no real unit cells. The shown structure is only one out of many possible proton disordered structures obeying the ice rules. In both pictures the a and c axes are shown. The third axis forms a 120° angle with the a and a 90° angle with the c axis. The proton order in the ice XI structure can be seen well, when compared to the ice Ih structure. The plot was done using the Jmol package [1].

T in K	κ in $\frac{\mathrm{W}}{\mathrm{m \cdot K}}$	T in K	κ in $\frac{\mathrm{W}}{\mathrm{m \cdot K}}$
10	120	120	5.4
15	60	150	4.3
20	38	200	3.2
40	16.1	250	2.4
80	8.1	273.2	2.14
100	6.5		

Table 1: Here the best estimate values for the thermal conductivity of ice Ih at atmospheric pressure computed by Slack [29] on the basis of several earlier experiments are shown. The uncertainty was estimated to $\pm 10\%$.

up to 145h at 89.4K.

The approximate degeneracy of the different proton configurations in proton-disordered ice leads to an additional entropy per molecule. It has been computed by Pauling [22] to be approximately

$$S_{\mathrm{hyd}} = k_{\mathrm{b}} \ln\left(\frac{3}{2}\right) \approx 3.494 \cdot 10^{-5} \frac{\mathrm{eV}}{\mathrm{K}}. \tag{7}$$

Pauling's computation did not take the possibility of rings into account. A more careful numerical derivation accounting for this possibility by using a series expansion was done by Nagle [21]. He found a value of $S_{\mathrm{hyd}} = (3.5333 \pm 0.0009) \cdot 10^{-5}\mathrm{eV/K}$, which differs only slightly from Pauling's original finding. In 1974 Haida et al. [13] did a careful experimental study. They compared the entropy of water vapor computed by following the entropy change heating ice from near 0K through melting and vaporization with the entropy calculated from spectroscopic measurements of the water vapor. The difference between those two values is the frozen-in residual entropy of the disordered hydrogen system. Their value of $S_{\mathrm{res}} = (3.52 \pm 0.23) \cdot 10^{-5}\mathrm{eV/K}$ agrees excellently with the value computed by Nagle.

2.2.2 Thermal Conductivity of Ice

The thermal conductivity of the different ice phases has been the objective of many studies. In 1980 Slack [29] used data from several sources to find

best estimate values for the thermal conductivity of ice Ih. His values are given in table 1.

The thermal conductivity of ice XI cannot be measured directly. Because of the slow relaxation time described in section 2.2.1 it is impossible to produce a sample of pure ice XI. Therefore, the doping method described above is used. Using that method, samples with approximately 68% ice XI were produced by Andersson and Suga [4]. By fitting their results to the Debye model they found the contribution of scattering by the dopant. Setting the fitting parameter for point defect scattering to zero allowed to get the thermal conductivity for pure ice. They verified this method by testing it on KOH-doped ice Ih. Comparing these values against experimental values for pure ice Ih, they found a good agreement.

The thermal conductivity of pure ice XI can then be found by use of a further model. Andersson and Inaba [3] used the effective medium approximation described in [15]. This allows to extrapolate the thermal conductivity of one substance in binary mixture with another substance when the thermal conductivity of the second substance and the mixture as well as the mixing ratio is known.

In 2005 Andersson and Inaba [3] published a summary of thermal conductivity values for various ice phases in form of a review article. Using data from several other publications they found power laws to describe the thermal conductivity of different ice phases. For ice Ih they concluded that later studies, for example by Andersson and Suga [4], backed Slack's findings. By using the additional data, they found the resulting values to agree well with the earlier results. Their estimate of the uncertainty of 5% for the temperature range 40-273K is only half as big as Slack's value, though. The ice XI data was taken from [4]. The parameterizations they found for the ice phases studied in this work at 0.1 MPa are:

$$\begin{aligned} \kappa_{\text{ice Ih}} &= \frac{632\frac{\text{W}}{\text{m}}}{T} + 0.38\frac{\text{W}}{\text{m}\cdot\text{K}} - 0.00197\frac{\text{W}}{\text{m}\cdot\text{K}^2}\cdot T \\ \kappa_{\text{ice XI}} &= 994\frac{\text{W}\cdot\text{K}^{0.041}}{\text{m}}\cdot T^{-1.041} \end{aligned} \tag{8}$$

The laws are valid for 40-273K for ice Ih and 50-72K for ice XI and have an inaccuracy given as 5% and 6% respectively. They also gave a simple power law for ice Ih but this is only valid up to 180K. The deviations above this temperature were ascribed to the increasing contribution of optical

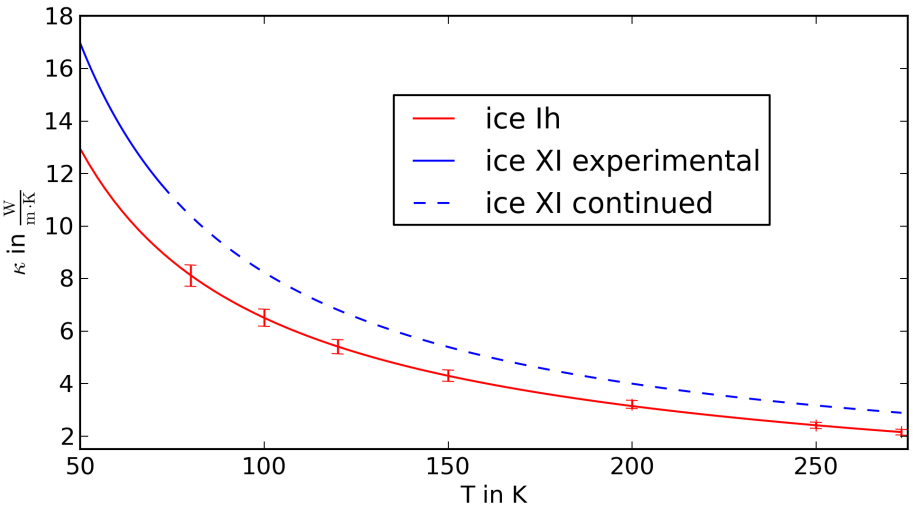

Figure 2: The parametrization of the experimental results for the thermal conductivity of the ices Ih and XI taken from [3] are shown. The data points correspond to the results by Slack [29] with uncertainties of 5% as given in [3]. The dashed line shows the continuation of the thermal conductivity parametrization for temperatures higher than the phase transition at 72K.

phonon scattering. The parameterization above includes this deviations and is therefore used as reference in this work.

For ice XI there are no experimental data for temperatures over 72K, since this is the transition temperature to ice Ih. The values received by simulations in experimentally unachievable regions are therefore compared against the power law in equation (8) even though its validity in this region is not known.

The anisotropy of the thermal conductivity of ice Ih has been shown to be of the order of 5% or less [29] at high temperatures[2] based on measurements on single crystals by Landauer and Plumb [17]. For ice XI there are no data on the anisotropy of the thermal conductivity because of the lack of a single crystal sample to measure. The data of Andersson and Suga [4] are found by measurements of polycrystalline ice. Therefore, their values are averaged over all directions.

[2]near 270K

The two parameterizations are plotted in figure 2. The blue dashed line is the continuation of the power law for the thermal conductivity of ice XI above the transition temperature. The data points included are the values found by Slack [29] with the smaller uncertainties argued for in [3]. The parameterization and the plotted best estimate values agree excellently.

2.2.3 Water models

In this work the thermal conductivity of ice is examined by using molecular dynamics simulations. The simulations are done using an empirical force field. One widely used empirical water model is the TIP4P/2005 model. It was proposed in 2005 by Abascal and Vega [2]. In this work a flexible version of this model, the TIP4P/2005f, proposed by González and Abascal [12], was used.

The TIP4P/2005 model is a four point model. In addition to the three sites defined by the oxygen (O) and the two hydrogen (H) atoms, there is a fourth site called M. This site carries the electric charge of the oxygen atom in the molecule. In the rigid case it is positioned in the molecular plane equally distant from the two H sites to retain the symmetry of the molecule and a distance of d_{OM} from the oxygen. The geometry of the H and O sites is set to match the experimentally measured structure. Since the molecules have to be charge neutral, the charge of the M site is minus two times the positive charge of the H sites. Both the rigid and the flexible model include the same type of intermolecular potentials. There is a Lennard-Jones interaction term between the O sites of different molecules, given by the usual form:

$$V_{\mathrm{LJ}} = 4\epsilon \cdot \left(\left(\frac{\sigma}{r_{\mathrm{OO}}} \right)^{12} - \left(\frac{\sigma}{r_{\mathrm{OO}}} \right)^{6} \right). \tag{9}$$

Additionally, there is an electrostatic interaction between the H and the M sites. The potential between site i in one molecule and site j in another molecule is given by:

$$V_{\mathrm{es}} = \frac{q_i q_j}{4\pi\epsilon_0 r_{ij}}. \tag{10}$$

The four parameters of the rigid model are σ, ϵ, q_{H} and d_{OM}. They were determined by tuning them to fit experimentally determined properties of

water and ice[3]. Later the flexible version TIP4P/2005f was introduced in [12]. It contains the same intermolecular potentials but it does not set the relative positions of the sites to a rigid geometry. Instead it introduces an intramolecular potential, which allows the bond lengths to fluctuate. This potential contains three parts:

$$V_{\text{intra}} = V_{\text{OH}_1}(r) + V_{\text{OH}_2}(r) + V_{\text{HOH}}(\theta). \tag{11}$$

The potential between the O and the H sites is modeled by a Morse potential. It is given by:

$$V_{\text{OH}_i} = D_{\text{r}} \cdot (1 - \exp(-\beta(r_{\text{OH}_i} - r_{\text{eq}}))^2. \tag{12}$$

In this work the quartic expansion of this potential is used, which is given by:

$$V_{\text{OH}_i} = D_{\text{r}} \left(\beta^2 (r_{\text{OH}_i} - r_{\text{eq}})^2 - \beta^3 (r_{\text{OH}_i} - r_{\text{eq}})^3 + \frac{7}{12} \beta^4 (r_{\text{OH}_i} - r_{\text{eq}})^4 \right). \tag{13}$$

The quartic expansion does differ only very slightly from the full Morse potential for the energies present in the simulations [12].

The angular potential is taken to be harmonic:

$$V_{\text{HOH}}(\theta) = \frac{1}{2} K_\theta (\theta - \theta_{\text{eq}})^2 \tag{14}$$

Because of the flexibility of the bond length, the position of the M site has to be redefined. Due to the symmetry of the molecule it will still be situated on the bisector of the HOH angle in the HOH plane. But the distance from the O site is redefined to be:

$$d_{\text{OM}} = d_{\text{OM}}^{\text{rel}} (r_{\text{OH}_1} + r_{\text{OH}_2}) \cos\left(\frac{\theta_{\text{HOH}}}{2}\right). \tag{15}$$

In the flexible case $d_{\text{OM}}^{\text{rel}}$ replaces d_{OM} as a parameter. Furthermore, five new parameters D_{r}, r_{eq}, β, θ_{eq} and K_θ are introduced. González and Abascal [12] determined the nine parameters of the flexible model to fit experimental data. They started from the parameters of the rigid model given in [2] and then varied them to fit the structure to the experimentally observed one[4]. In this work these parameters are used. The values are given in table 2.

[3]For details refer to [2].

[4]For details refer to [12]

Parameter		Value	Parameter		Value
σ	[Å]	3.1644	D_r	[kJ/mol]	432.581
ϵ/k_b	[K]	93.2	r_eq	[Å]	0.9419
q_H	[e]	0.5564	β	[nm^{-1}]	22.87
$d_\mathrm{OM}^\mathrm{rel}$		0.131 94	θ_eq	[°]	107.4
			K_θ	[$\mathrm{kJ/mol/rad}^2$]	367.810

Table 2: The values for the parameters of the TIP4P/2005f model are taken from [12]. The parameters were constructed there starting from the rigid model defined in [2]. The values of the additional five parameters on the right were then tuned to fit experimental properties.

3 Simulation Method

In this work the empirical force-field model described in section 2.2.3 is used for a non-equilibrium molecular dynamics simulation to investigate the influence of proton order on the thermal conductivity on water.

3.1 Non-Equilibrium Molecular Dynamics

In contrast to Monte Carlo methods, molecular dynamics samples the phase space by following the system through time. By modeling the time evolution of the system the method is suitable to analyze the dynamical properties of a system. By forcing the system out of equilibrium one can directly measure for example transport properties of a system.

This way of measuring transport properties is called the "direct method". In this work it will be used to measure the thermal conductivity of various ice cells. By varying the system, as for example by introducing defects or enforcing experimentally unavailable geometries, this method allows to examine their influence on the thermal conductivity in an isolated way.

To measure the thermal conductivity, the system has to be forced into a non-equilibrium state. This can be done in two different ways:

- Introducing a thermal gradient by thermostating two regions of the cells to different temperatures:

  These different temperatures enforce a temperature gradient in the simulation box which leads to a heat flux throughout the cell. Measuring this flux by monitoring the velocities and energies of the particles, the thermal conductivity can be evaluated.

- Introducing a heat current in the system:

  When energy is transfered constantly from one region of the system to a second one, a thermal gradient will build up. In the steady state this thermal gradient becomes constant and by measuring it the thermal conductivity can be evaluated as well.

In 1997 Müller-Plathe [20] suggested that the second method is better suited to find the thermal conductivity by simulation. He claims that the thermal gradient converges much faster than the heat flux. Therefore, by imposing the heat flux and measuring the thermal gradient the system will

converge faster, allowing shorter runs and a better averaging. Because of these advantages the second method is used in this work. The heat flux is introduced by the switching algorithm suggested in [20].

The algorithm was implemented and then used in a preexisting simulation package, which is described below.

3.2 Simulation Package

All simulations in this work are done using the arce package by Ramirez [24]. This software package allows molecular dynamics and Monte Carlo simulations. In this work only the molecular dynamics functionality is used. Even though the package allows path integral molecular dynamics (PIMD), this feature is not used in this work. All simulations are done treating the hydrogen cores classically which corresponds to PIMD with one bead.

A major advantage of the package are its modules to do simulations of water and ice. Specifically it has modules for the classical force field models of the TIP4P type described in section 2.2.3 with either rigid or flexible molecular geometry. As described above, in this work, the TIP4P/2005 models flexible version with the parameters from table 2 is used.

As is customary in such simulations, periodic boundary conditions are applied to minimize the finite size effects in the simulation. The Lennard Jones potential is cut off after half of the cell size whose thermal conductance is measured. The long range terms in the potential cutoff are smoothened by a uniform tail correction.

For the electrostatic forces the long range term cannot be neglected. Therefore, a particle mesh Ewald method is used. This method collects the sum over all pair potentials into two separate sums. The short range terms are summed in real space. This real space sum is cut off after 8Å. To account for the long range terms an additional sum in Fourier space is performed. The long range sum in Fourier space converges quickly compared to doing a sum in real space. Nonetheless, the reciprocal Ewald sum is the computationally most expensive task of the simulation. Therefore, the presence of electrostatic forces only allows shorter runs of smaller cells than for example in the studies [28] and [35] using a similar method on Silicon.

The integrators used within the package were derived by Martyna, Tuckerman, Tobias, and Klein [19]. For the NVE ensemble, a velocity-Verlet algorithm is used. The equilibrations are done in the NPT ensemble. To enforce the temperature, the system is coupled to a Nose Hoover chain of length

four. To pressurize the system to the right value, the cell size is allowed to fluctuate isotropically and the system is coupled to another barostat degree of freedom.

For the production runs the thermostats are turned off and therefore the cell size is fixed again. The run now uses the velocity-Verlet integrator. Nonetheless, it is not in the NVE ensemble since now the system is forced out of equilibrium.

3.3 Switching Algorithm

In all runs, the cell geometry shown in figure 3 is used. Periodic boundary conditions are applied in all three directions. The cell has two short sides along the x and y direction, and a long side along the z direction. At least 14 strips are introduced along the z direction of the cell. By calculating the temperature in each strip, the temperature profile along the z direction can be computed. The temperature in each strip is estimated as the kinetic temperature of the molecules whose center of mass (com) is in the strip. The kinetic temperature in strip n, T_n, is found, similarly to [20], as:

$$\begin{aligned} T_n &= \frac{2\overline{E_{\mathrm{kin,n}}}}{3N_n k_{\mathrm{b}}} \\ &= \frac{m_{\mathrm{H_2O}}}{3N_n k_{\mathrm{b}}} \sum_{i \in n}^{N_n} v_{i,\mathrm{com}}^2, \end{aligned} \tag{16}$$

where the sum is performed over all N_n molecules in the n^{th} strip. This estimation is based on the assumption of local equilibrium. According to the equipartition theorem, in equilibrium all degrees of freedom will carry the same average energy. Therefore, averaging only over the three translative degrees of freedom of each molecule will give a good temperature estimation.

The heat flow is introduced by the velocity switching suggested in [20]. All equations following in this chapter are based on his work. The same method has also been used in simulations of liquid water for example by Bedrov and Smith [6]. The center of mass (com) velocity of the fastest and therefore "hottest" molecule i in the cold strip v_i^{com} is changed with the com velocity of the slowest and therefore "coldest" molecule j in the hot strip v_j^{com}:

$$\begin{aligned} \vec{v}'_{i,X} &= \vec{v}_{i,X} - \vec{v}_{i,\mathrm{com}} + \vec{v}_{j,\mathrm{com}} \\ \vec{v}'_{j,X} &= \vec{v}_{j,X} - \vec{v}_{j,\mathrm{com}} + \vec{v}_{i,\mathrm{com}}, \end{aligned} \tag{17}$$

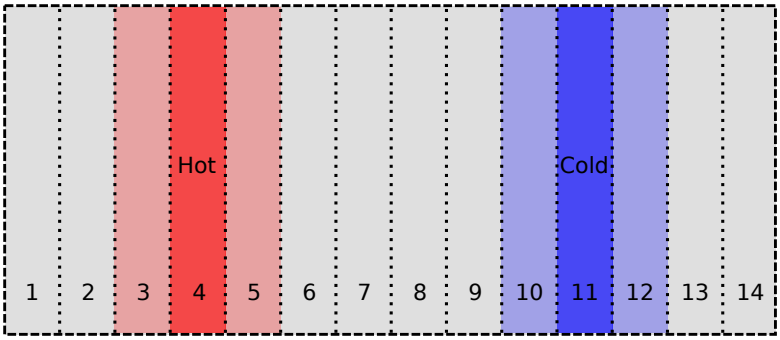

Figure 3: A schematic picture of the cell geometry is shown. Periodic boundary conditions are applied. By switching the center of mass velocity of the fastest molecule in the *cold* strip (11) and of the slowest molecule in the *hot* strip (4) a heat flow is introduced. The temperature in each strip is estimated by monitoring the average kinetic energy of the molecules in each strip. To estimate the temperature gradient the reservoirs (4 and 11) and their direct neighbors (3, 5, 10 and 12) are not taken into account.

where i, X denotes the 3 atoms X of molecule i.

This will introduce energy in the hot reservoir and drain the same amount of heat from the cold reservoir. The energy difference is given by:

$$\begin{aligned} E_{\text{switched}} &= E'_{\text{kin}} - E_{\text{kin}} \\ &= \sum_{i=1}^{3} \frac{m_i \vec{v}_i'^2}{2} - \sum_{i=1}^{3} \frac{m_i \vec{v}_i^2}{2} \\ &= \sum_{i=1}^{3} \frac{m_i (\vec{v}_{i,\text{rel}} + \vec{v}'_{\text{com}})^2}{2} - \sum_{i=1}^{3} \frac{m_i (\vec{v}_{i,\text{rel}} + \vec{v}_{\text{com}})^2}{2} \\ &= \frac{m_{\text{H}_2\text{O}}}{2} (\vec{v}'^2_{\text{com}} - \vec{v}^2_{\text{com}}) + \frac{\vec{v}'_{\text{com}} - \vec{v}_{\text{com}}}{2} \sum_{i=1}^{3} m_i \vec{v}_{i,\text{rel}} \\ &= \frac{m_{\text{H}_2\text{O}}}{2} (\vec{v}'^2_{\text{com}} - \vec{v}^2_{\text{com}}), \end{aligned} \tag{18}$$

where the sum always goes over the three atoms in the molecule taking part in the switching. In the last step the definition of the com velocity was used

($\sum_i m_i \vec{v}_{i,\mathrm{rel}} = 0$). Obviously the energy drain and gain are equal. Therefore, the overall energy is conserved. This has similarly been shown in [6].

The com velocity is switched instead of switching the velocity of all atoms of the molecule separately to prevent any unwanted effects on the structure of the ice. The molecules will have different orientations and different surroundings. Therefore, switching the atomic velocities could cause problems in the molecular and crystal structure. This is prevented by switching the com velocities instead.

Switching regularly introduces a heat transfer from the cold to the hot strip. The switching is repeated regularly but not at every time step. As Müller-Plathe [20] found, it is necessary to allow the system to rethermalize after a switching event. By waiting a certain amount of steps between the switches, one allows the velocities of the molecules in the reservoir strips to regain a broad distribution. This ensures that the fastest molecule in the cold strip is always faster than the slowest molecule in the hot strip, and therefore the heat flow is always directed in the same direction.

A steady state is reached, when all energy transported by the switching is canceled by the heat flux from the hot to the cold region and the average temperature gradient does not change anymore. Only thermal fluctuations will be present. The heat flux through the system is then given by [20]:

$$\begin{aligned} J &= \frac{1}{2} \cdot \frac{E_{\mathrm{switched}}}{A\ \Delta t} \\ &= \frac{m_{\mathrm{H_2O}}}{4A\ \Delta t} \cdot \sum_{\mathrm{switchings}} (v_{i,\mathrm{com}}^2 - v_{j,\mathrm{com}}^2), \end{aligned} \tag{19}$$

where A is the cross-sectional area of the cell and Δt is the time over which the switchings are conducted. The factor one half arises from the fact, that the energy can be transported two ways, due to the periodic boundary conditions and the cell geometry shown in figure 3.

If the heat flux and the thermal gradient are known, the thermal conductivity along the z direction can be computed as defined in equation (2) [20]:

$$\begin{aligned} \kappa &= -\frac{J}{\partial_z T} \\ &= -\frac{m_{\mathrm{H_2O}}}{4A\ \Delta t\ \partial_z T} \cdot \sum_{\mathrm{switchings}} (v_{i,\mathrm{com}}^2 - v_{j,\mathrm{com}}^2). \end{aligned} \tag{20}$$

The switching algorithm is easy to use and to implement and as stated in [20] obviously conserves the total momentum of the cell. This is very important since an overall drift of the cell has to be prevented. The overall energy is also conserved. The positions remain unchanged, which leads to conserved potential energy. Since all molecules have the same mass, switching the com velocities of two molecules will conserve the kinetic energy.

The angular momentum of the cell is not necessarily conserved [20]. Therefore, the velocity switches could lead to a turning of the cell. But the amount of angular momentum that can be introduced with one switch is rather small. Also averaging over many switching events during the simulation will further decrease this effect.

There have been other algorithms proposed and used to introduce a heat flux in the system. Most are working by velocity rescaling. This would allow the heat flux to be set constant to one specific value. This is not necessary since the thermal conductivity is not dependent on the heat flux through the system as long as it is small enough to stay in a linear response regime. Also simple velocity rescaling will scale the relative velocities of the atoms in the molecules as well. This could lead to unwanted effects. Because of this and the simplicity of the switching algorithm, it is used in this work.

3.4 Finite Size Effects

Due to the small system size, ballistic heat transport is a dominant contribution to the heat flux. For small systems the main part of the heat conduction is ballistic transport from one reservoir to the other. This has been found for example in a study by Schelling et al. [28]. They argue that the average mean free path for ballistic heat transport l_{res} is given by half the distance between the reservoirs. If this is smaller or of the same order as the mean free path for the other scattering mechanisms, the thermal conductivity given by equation (20) will differ notably from the bulk limit, which is found in experimental studies. To extrapolate the bulk limit from the values found in simulations for different cell lengths, they used Matthiessen's rule as given in equation (6). The same method is used in this work.

In the Debye model the thermal conductivity is proportional to the effective mean free path of the phonons as seen in equation (5). Using Matthiessen's

rule to find the effective mean free path, Schelling et al. [28] found:

$$\kappa \propto l_{\text{eff}} = \left(\frac{1}{l_{\text{res}}} + \frac{1}{l_{\text{bulk}}} \right)^{-1}. \tag{21}$$

As expected the bulk limit is recovered by taking l_{res} to infinity:

$$\kappa_{\text{bulk}} = \lim_{l_{\text{res}} \to \infty} \kappa. \tag{22}$$

Since the thermal resistivity κ^{-1} is proportional to the inverse of the effective mean free path, its bulk limit can be extrapolated by taking l_{res}^{-1} to zero, doing a linear extrapolation [28]. If the thermal conductivity is known for multiple cell lengths, then in a linear fit of the thermal resistivity against the inverse cell length, the bulk thermal resistivity will be given by the y axis interception of the fit.

To do a decent extrapolation, many data points are needed. The bulk mean free path is of the same order of magnitude as the cell lengths considered in this work. Having much longer cells is computationally not manageable. Therefore, even when the uncertainties of the different data points corresponding to the simulation of one cell length are reasonably small the uncertainty of the extrapolated value will still be large. Nonetheless, the extrapolation is useful to compare the results of the simulation to experimental findings. On the other hand many interesting properties can already be seen by comparing cells of the same length with different properties.

3.5 Parameters of the Switching Algorithm

For the simulation runs there are several parameters to set. The most important ones are:

- Switching Frequency:

  The number of steps between two switching events determines the size of the heat current introduced into the system. The number of pausing steps has to be chosen large enough to allow the reservoir strips to rethermalize between switches. Also switching too often can lead to unwanted waves in the system.

  Nonetheless, the gap between switches should not be too large either. If the number of switches is too small, the thermal fluctuations in the heat flux and the thermal gradient will lead to large uncertainties.

By simulating systems with different switching frequencies, it is found that valid frequencies lie between 300 and 700 steps per switching. Most simulations are done with a 600 steps gap. Some runs are done using 300 and 500 steps instead.

- Number of Strips:

  The number of strips in the system should be chosen large enough to allow a decent linear fit. The temperature profile of the cell is not linear over the whole z range. Especially for high heat fluxes, there are peaks in the temperature of the reservoirs. The linear fit is done in the middle between the two reservoirs. To allow a decent fit at least four points should be included. Therefore, the minimum number of strips is 10.

  To ensure that the fit is done in the linear regime, a buffer strip on each side of the reservoirs was included. For this 14 strips are needed. This allows a decent linear fit and therefore this number was used for most calculations.

  Increasing the strip number even further decreases the number of molecules per strip. This increases the statistical fluctuations in the temperature averaging. Some runs are using 18 strips in the system. Higher numbers have not been considered.

- Cross-sectional Area of the Cell:

  The size of the cell also has to be chosen carefully. To allow a decent extrapolation, cells with a large distance between the reservoirs are needed. To allow long cells, the cross-sectional area has to be sufficiently small. Otherwise the number of molecules in the cell will increase too much, leading to unfeasibly long simulation runs.

  On the other hand choosing the cross-sectional area too small may cause additional finite size effects. Also enough molecules per strips are needed to decently define the temperature of the strip.

3.6 Details of the method

In addition to these parameters, also the parameters of the molecular dynamics have to be set. In this section the details of the used method and

the evaluation of the results are explained. First details of the simulation performed are described. Afterwards the evaluation methods are listed.

3.6.1 Details of the Simulation Method

All simulations in this work are done using the package and algorithms described in section 3.2. For the non-equilibrium runs the switching algorithm described in section 3.3 was added to the arce package. Also the temperature estimation of the different strips was implemented. Otherwise, the package was not changed.

For all simulations a time step of 0.5fs is used. The temperature is written out every 25^{th} step. The pressure is monitored every 10^{th} step. To do a run for one cell the following procedure is performed.

The cells are first equilibrated in an NPT run to the corresponding temperature and 0.1MPa pressure by allowing the cell size to fluctuate isotropically. After 50-100ps of equilibration, the cell size is fixed and the thermostat is switched off. Since there are fluctuations in the pressure even in the pressurized system, fixing the last system size leads to different average pressure values for the different cells. The pressure is not 0.1MPa on average. Nonetheless, this method is used. Due to the switching the pressure in the system will change during the non-equilibrium simulation for all initial system sizes. Furthermore, the influence of the pressure on the thermal conductivity is much smaller than the statistical uncertainties arising from the thermal fluctuations. This has been found for example by Andersson and Suga [4]. Because of that, no further effort is made to reach a certain pressure in the system.

After the equilibration the switching is turned on and the simulation is run in the non-equilibrium regime for 200ps or more. For some of the smaller cells with a smaller heat flux simulation times of up to 500ps are reached. For three runs only times of 150ps or 175ps are simulated. Due to the rather high heat flux in these cases the steady state was reached rather early. Long runs are necessary to reach the steady state in the system. Both the temperatures of the strips and the heat flux fluctuate strongly. Especially the temperatures in the small cells are found by averaging over just around 25 molecules. Also only the "hottest" and "coldest" molecules out of a pool of 25 molecules in the cold and hot reservoir are chosen for the switching. Therefore, large fluctuations are expected. For the longer cells the averaging works better but still around 100-200ps are needed to reach the steady state which in turn

leads to very short averaging times.

Generally higher heat fluxes reduce the relative size of the fluctuations and therefore allow shorter simulation runs. Most of the early runs were done with high heat currents and relatively short simulation times. The later runs are done with a lower heat current but a longer simulation time, because of the temperature differences between the two reservoirs becoming rather large for the high heat currents. But since the values for both types of runs agree very well also the earlier runs are taken into account in the evaluation.

3.6.2 Details of the Evaluation

To find the thermal conductivity in the different cells, the temperature of the strips is monitored in combination with the switched energy per time step. Using these quantities, the beginning of the steady state is found. The usual point for this was after 200ps for the low heat flux and 100ps for the higher heat flux. Especially the short cells showed large thermal fluctuations, which tended to delay the start of the steady state.

An example of the time evolution of the strip temperatures during the switching is shown in figure 4. The shown plot had to be smoothened by a moving window average. Because of the large thermal fluctuations otherwise the overall time evolution would not be visible. The window size is set to 4000. Therefore, each data point in the plot shows the average of the last 50ps. The average leads to a misrepresentation of the first steps. It cannot be seen in the plot that all strips start at roughly the same temperature. After the sharp increase of the temperature gradient during the first 50-100ps the convergence gets slower. In this run the steady state is considered to start after 200ps (400000 steps).

Especially for smaller cells large fluctuations make it difficult to find the start of the steady state. This is no major problem because for shorter cells longer runs are feasible and available. Therefore, the averaging can be started at a later point in the run without loosing the necessary statistics. Runs that did not reach a steady state are excluded from the evaluation. One cause for this is the running time being too short. But also runs with smaller cells are excluded, when the thermal fluctuations are too big to determine the start of the steady state. An example for an excluded run is shown in figure 5.

Especially for shorter cells there are many large fluctuations or temperature jumps that prevent the system to reach the steady state. Also several runs have not been performed for a long enough time. Therefore, the number

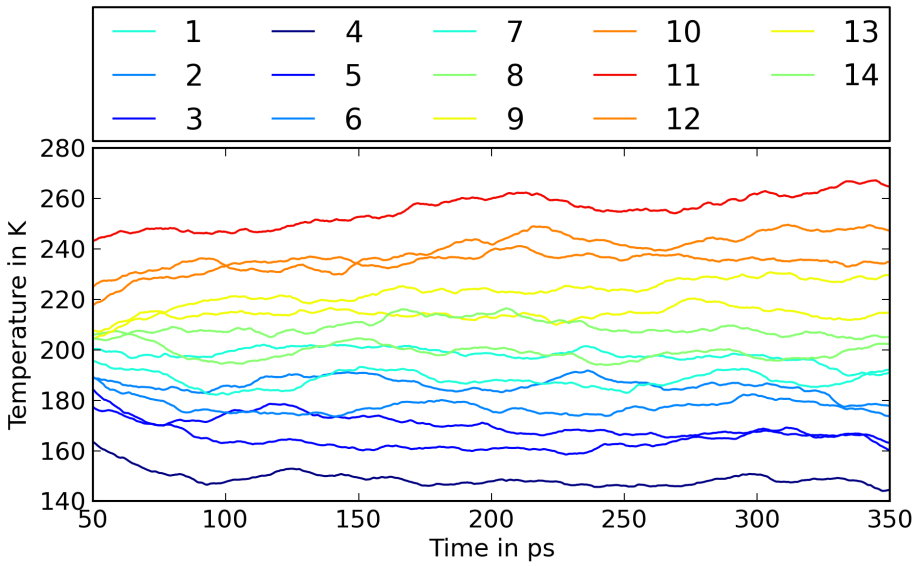

Figure 4: Here the time dependence of the strip temperatures is shown. There are huge thermal fluctuations due to the small number of molecules in each strip and due to fluctuations in the heat current. To make the long time evolution visible the graph is smoothened using a windowed average over 4000 data points (50ps). Therefore, each data point corresponds to an average over the previous 4000 temperatures. In this case the steady state is taken to set in after 200ps.

of excluded runs is rather large.

Because of the large fluctuations in both the switched energy and the temperature of the strips, the starting point of the steady state is set in a way to capture the most constant part of the run. This is done by including all corresponding features of the two values. In some cases relatively large fluctuations in the heat flux result in a fluctuation of the temperature profile. In these cases the starting point is set to exclude both features.

The method of determining the start of the steady state is rather subjective. It depends on the appearance of the time evolution of the strip temperatures and the resulting temperature profile. A better method would be to find the time after which the temperature does not change noticeably. A similar evaluation has been done by Zhou et al. [35] for their examination of Silicon. Unfortunately this method is not realizable in the present

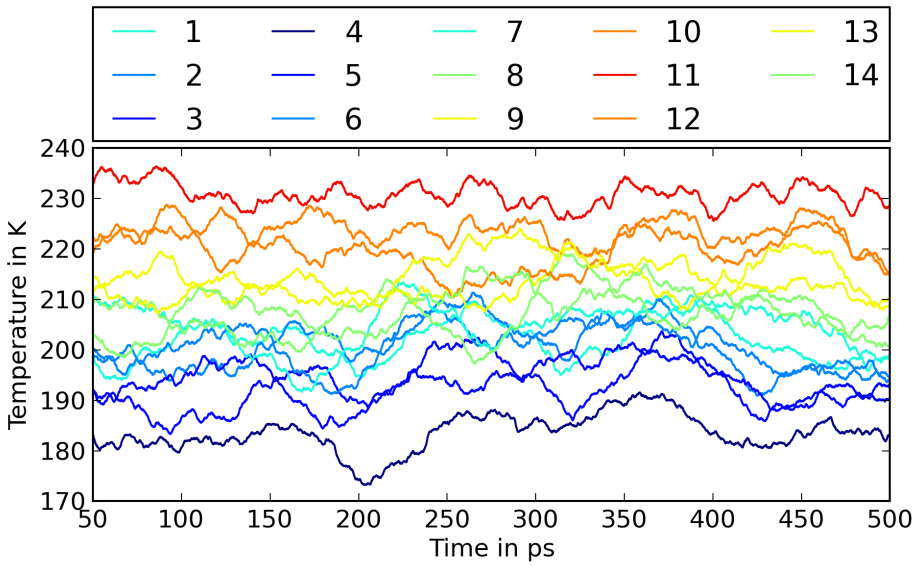

Figure 5: In this plot the time evolution of the strip temperatures for an unconsidered run is shown. As in figure 4 the graph is smoothened using a windowed average over 400 data points (50ps). The fluctuations, especially in the low temperature strips, even in the heavily smoothened graph are much too big to determine a possible steady state.

case. The switching algorithm does not introduce a constant heat flow but is subject to statistical fluctuations on a long time scale (up to 100ps) of up to $\pm 5\%$. These are assumed to average out over the whole steady state area. Nonetheless, the time intervals that are compared to find the beginning of the steady state would have to be rather long. This is not possible due to the long simulation times. Therefore, due to the lack of alternatives the manual version of determining the start of the steady state is used in this work. Nonetheless, this method definitely leaves room for improvements in future studies.

After the starting point is found, the temperature of the strips is determined by averaging over all later temperatures. This is done using a Gaussian fit. Since the strip temperature is found by averaging over the kinetic energy of all molecules in a strip a Gaussian distribution of temperature values is expected for the different strips.

The temperature is only measured every 25^{th} step, to get roughly indepen-

dent values. A histogram is produced by separating the temperature interval into 201 bins. The error on the number of values in each bin is simply given as the square root of the corresponding bin count. Then a Gaussian function is fit to the distribution. The fit parameter for the center of the distribution is taken as the temperature of the strip. The uncertainty is estimated by the square root of the corresponding diagonal entry in the covariance matrix as given by the scipy [16] method optimize.curve_fit. To this value, half of the bin size is added to account for the uncertainty resulting from the discretization.

The thermal profile obtained by that method is used to find the thermal gradient. The positions of the strips are taken as the distance of the strips center from the center of the hot bath. Because of periodicity of the cell as seen in figure 3 there are two data points for every separation. The only exception are the reservoirs with zero separation for the hot region and the maximum possible separation of half the length of the cell for the cold region.

Due to thermal fluctuations the two data points for the different directions do not perfectly match in most cells. To find a good estimate of the average thermal gradient in the cell the mean of the two values is taken. The uncertainty of the resulting value is then taken as half of the distance of the two data points plus the square root of the added squares of the uncertainties of the single data points.

The resulting four data points are fitted with a linear function using the same scipy method optimize.curve_fit as for the Gaussian fit above. Again the uncertainty is estimated as the square root of the covariant matrix diagonal entries returned by the fitting function. This can lead to an underestimation of the uncertainties, when the data points lie well on a line by chance. The fit method does not account for the size of the uncertainties other than using them as weights. An alternative way of doing the fit would be for example a bootstrapping algorithm. To do a decent bootstrapping fit good knowledge of the uncertainties of the data points are needed. The method described above only gives an upper bound on the uncertainties. Therefore, the curve_fit method tends to give better results. It is therefore used for the temperature gradient fit.

The heat flux is computed by use of equation (19). The amount of energy switched for each switching event is taken to be independent due to the large gaps between the switches. Therefore, the uncertainty of the energy transfered by one switching is estimated by the standard deviation of the switched energy divided by the square root of the number of values. Multiplying this

by the number of switchings gives the uncertainty of the overall switched energy $\Delta E_{\text{switched}}$. The uncertainty in the time interval $\Delta(\Delta t)$ of the heat flux is taken to be the time gap between two switches. The uncertainty in the heat flux is then given as:

$$\Delta J = \frac{E_{\text{switched}}}{4A\Delta t}\sqrt{\left(\frac{\Delta E_{\text{switched}}}{E_{\text{switched}}}\right)^2 + \left(\frac{\Delta(\Delta t)}{\Delta t}\right)^2}. \tag{23}$$

Using the computed values for the heat flux and the temperature gradient the thermal conductivity is computed using Fourier's law (1). The two variables are obviously correlated. Therefore, in an estimation of the uncertainty the covariance terms cannot be neglected. To get an estimate of the uncertainty of the resulting value, the relative uncertainties of the two values are added. The resulting uncertainty for the thermal conductivity is given by:

$$\Delta\kappa = \frac{J}{\partial_z T}\left(\left|\frac{\Delta J}{J}\right| + \left|\frac{\Delta(\partial_z T)}{\partial_z T}\right|\right). \tag{24}$$

To get an estimate of the bulk value of the thermal conductivity an extrapolation has to be done as described in section 3.4. For the extrapolation to work several cells of different lengths have to be simulated. Then a linear fit is done for κ^{-1} against l_z^{-1}. The resulting y axis intercept then corresponds to an infinitely large cell. This gives an estimate of the bulk thermal conductivity.

The fit is done using a bootstrap method similar to the one suggested by [35]. This method tries to correctly resample the data. 10000 new data sets are produced on the basis of the old data set and the knowledge of its uncertainties. To do this a Gaussian distribution is assumed for all data points. The standard deviation of the distribution is set to the estimated uncertainty. Then for every point a random deviation from the middle value based on the corresponding distribution is found by the numpy [32] method random.normal.

For each data set a least square fit is done using the scipy method optimize.leastsq. The best estimate for the fit parameters and their uncertainties is then found by taking the arithmetic mean and the standard deviation of the parameter values found for all 10000 data sets. This extrapolation method allows to get an estimate of the uncertainties for $\kappa_{\text{bulk}}^{-1}$ on the basis of the

uncertainties of the single cells. If their uncertainties are well estimated the extrapolated value and its uncertainty will be fairly well predicted.

The uncertainty of κ_{bulk} can then simply be found by uncertainty propagation. This result will be a good estimation as long as the relative uncertainty of the resistivity is not too large. If the relative uncertainty becomes too large, the linear approximation used in the uncertainty propagation breaks down. This does not happen for all but one extrapolation. Therefore, the uncertainty propagation is considered valid unless it is explicitly stated otherwise.

3.7 Production of the Ice Cells

For the simulation runs ice crystals of different sizes and structures have to be produced. To produce the ice XI cells a unit cell of four molecules, provided by Marivi Fernandez-Serra, is periodically repeated to obtained the desired size. The lattice constants are assumed to be equal to those used for the proton ordered ice Ih. The oxygen atoms then are at the same positions as for the ice Ih cells but the proton structure is ordered corresponding to the ice XI structure.

For the ice Ih cells the ice_gen code by Marivi Fernandez-Serra is used. Since ice Ih has a proton disordered structure, there is no unit cell which can simply be repeated. To achieve such a disordered structure, the ice_gen code first sets the oxygens onto the lattice, by repeating a four molecule unit cell. Each oxygen has four possible hydrogen sites. Two hydrogens are now distributed randomly onto these four sites. By doing that, the ice rules will obviously be violated at first. Now a Monte Carlo method is used to obtain an allowed structure.

To get an unordered structure, this method is repeated 100 times. Then the structure with the lowest overall dipole moment is selected. Since an ice Ih crystal has no dipole moment and ice XI is a ferro electric material, the overall dipole moment is an order parameter. The cell with the lowest dipole moment is therefore considered the "most unordered".

4 Simulations and Results

The main goal of this work is to examine the thermal conductivity of proton-ordered and unordered ice at different temperatures. For this, proton-ordered and unordered cells are examined at 100K, 150K and 200K. Smaller temperatures are not considered, since the mean free path of the phonons increases rapidly with decreasing temperature. To get a decently extrapolated bulk value for low temperatures, very large cells would be needed. This cannot be done in a decent time.

Furthermore, the introduction of defects in the cell and their influence on the thermal conductivity is examined. Also some simulations are done to verify the validity of parameters chosen in the simulation.

4.1 Check of the Method

To verify that the chosen cells allow to get a good understanding of the present mechanisms, several runs are done comparing different possible cells. The cross-sectional area of one cell is varied to ensure that it does not have any influence on the thermal conductivity measured for a certain temperature and cell length. Furthermore, runs are performed to examine the influence of the dipole moment of the cell on its thermal conductivity.

4.1.1 Cross-Sectional Area

To verify that the cross-sectional area does not influence the thermal conductivity, an unordered cell with a cross-sectional area of three by five unit cells ($\approx$ 13.5Å by 22.6Å) is compared to results of the corresponding run with a three by three unit cells ($\approx$ 13.5Å by 13.5Å) cross-sectional area. The latter is used for most of the other production runs. The two values are given in table 3. They agree very well. Therefore, the cross-sectional area is taken to have no influence on the thermal conductivity measurements. Because of that, it is valid to use the smaller cross-sectional area, which allows longer cells and longer runs due to the smaller number of molecules.

4.1.2 Non-Zero Dipole Moment

When constructing the unordered cells using the method described in section 3.7, it turns out that for cells with a cross-sectional area of three by three

A	l_z [Å]	κ [W/m/K]	$\bar{T}$ [K]	$\bar{p}$ [MPa]	gap
3x3	116.6	1.25±0.07	102.90±0.02	−48.2±0.4	300
3x5	116.6	1.24±0.06	100.94±0.02	−27.2±0.3	600

Table 3: The results for two unordered cells of the same length with different cross-sectional areas at 100K are shown. In both cases 14 strips were introduced. The resulting thermal conductivities agree excellently. "gap" is the number of steps between two switching events.

unit cells, the dipole moment never reaches near zero values. Otherwise this cross-sectional area is considered optimal. It is large enough to have enough molecules in each strip even for short cells. Also it does not seem to induce any additional finite size effects. On the other hand it is sufficiently small to allow long cells, which are needed to extrapolate to the bulk limit.

To check whether this cross-sectional area produces any significantly different results from a cell with near zero dipole moment, cells with a cross-sectional area of three by four unit cells are examined. Two types of cells are simulated. For the first type the dipole moment is minimized as described in section 3.7. This leads to cells with no significant dipole moment. These cells are considered totally disordered. To see if the dipole moment has any significant influence on the thermal conductivity, the second type of cell is produced in the same way but with maximized dipole moment along the c axis. This cells are called partially ordered.

For each type of cell, five cells with different lengths in the c direction are examined. All simulations are done at 100K. This is the lowest temperature considered in this work. For low temperatures the difference between ordered and unordered ice increases, as seen in figure 2. Therefore, the differences between unordered, partially ordered, and ordered cells should be biggest for this temperature. By doing the simulations as described in section 3.6, the results given in table 4 are obtained.

In the plot of the results, shown in figure 6, one sees, that there are some deviations between the cell types. Generally the uncertainties of the near zero dipole moment cells seem to be underestimated a little. But overall there is no systematic trend in the differences between the two cell types.

Therefore, one can obtain the thermal conductivity of ice Ih by simulating cells produced with ice_gen, even when they do not reach near zero dipole moment. It seems that it is not possible to get cells with significant partial

Near Zero Dipole Moment:			
l_z [Å]	κ [W/m/K]	$\bar{T}$ [K]	$\bar{p}$ [MPa]
87.4	0.94±0.04	100.80±0.02	−6.2±0.3
102.3	1.22±0.04	99.76±0.02	−33.2±0.3
116.4	1.42±0.06	100.10±0.02	27.3±0.3
131.0	1.33±0.05	100.48±0.02	14.4±0.3
145.5	1.53±0.04	100.02±0.01	27.5±0.2
Maximized Dipole Moment:			
l_z [Å]	κ [W/m/K]	$\bar{T}$ [K]	$\bar{p}$ [MPa]
87.6	1.12±0.11	102.91±0.02	−89.7±0.3
102.0	1.10±0.08	100.64±0.02	−13.8±0.3
116.6	1.26±0.10	102.03±0.02	−14.8±0.3
131.0	1.56±0.07	99.45±0.01	18.7±0.3
145.7	1.60±0.07	100.18±0.01	−19.3±0.3

Table 4: These are the results for an unordered cell with near zero dipole moment and dipole moment maximized along the c direction. All simulations are first equilibrated to 100K and 0.1MPa. All cells contain three by four unit cells in the a/b direction ($\approx$ 13.5 by 18.1 Å). The switching is done every 600 steps (300fs).

ordering using that method.

Most cells examined in this work have a cross-sectional area of three by three unit cells. This does not allow a near zero dipole moment but as shown above this does not cause any deviations. From here on, these cells will be called unordered. Having this relatively small cross-sectional area allows to simulate much longer cells and therefore to get closer to the bulk limit.

The method seems to give consistent results. The results for the different cell types examined in this work are given in the next sections. Most of the runs are done along the c direction of the crystal. This is justified by the lack of anisotropy found in experimental studies as described in section 2.2.2. To verify that this is reproduced by the simulation runs along the a/b direction are done for comparison. But as long as it is not indicated otherwise, all following results are obtained along c direction.

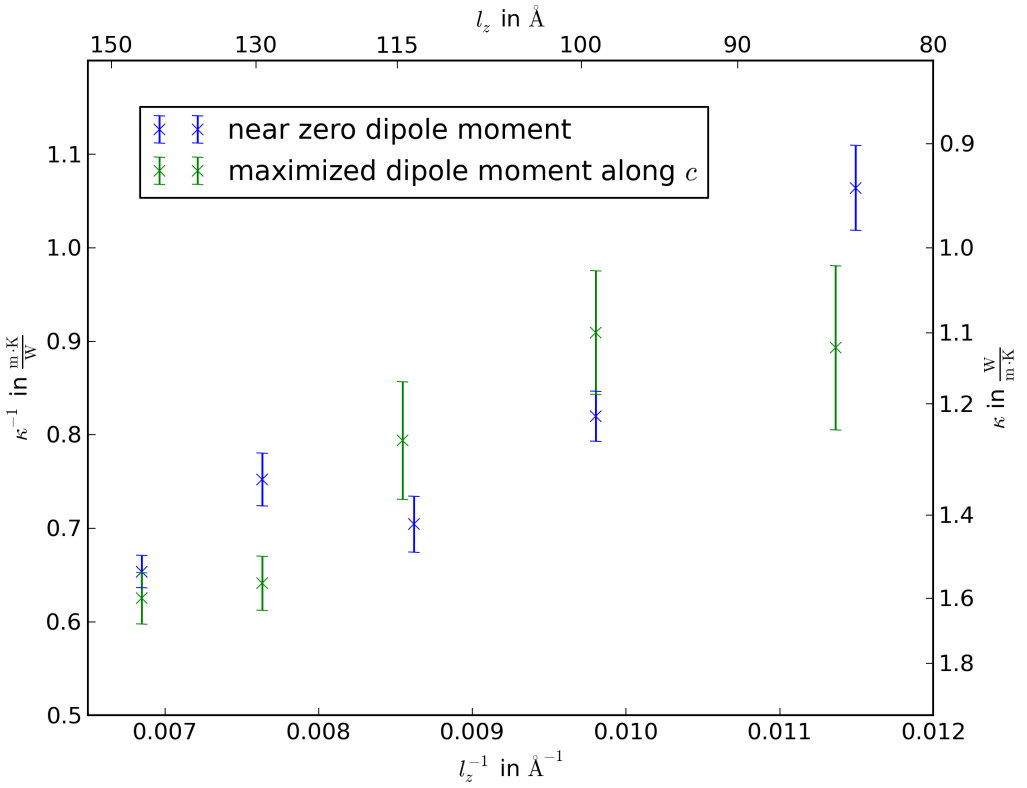

Figure 6: The thermal conductivities of cells with near zero dipole moment and a dipole maximized along the c direction using the ice_gen code are shown. Statistical fluctuations are visible, but there is no systematic difference between the two cell types.

4.2 Unordered Ice Ih

In this section the results for all unordered cells are presented. First the results along the c direction are shown. Here the cross-sectional area is taken to be three by three unit cells. As mentioned in the last section, this leads to a non-zero dipole moment of the cell. But as described in section 4.1.2, this does not affect the results in any significant way. Therefore, the results in this section are considered unordered regardless of their dipole moment.

Three different temperatures are examined. There are runs for 100, 150 and 200K. The results are shown in tables 5, 6 and 7 respectively. The data was found following the evaluation procedure described in section 3.6.2. The

Unordered Cells at 100K along c:					
l_z [Å]	κ [W/m/K]	$\bar{T}$ [K]	$\bar{p}$ [MPa]	n_{str}	gap [fs]
72.8	0.95± 0.04	97.02±0.02	44.3±0.5	14	150
87.4	1.12± 0.06	97.85±0.02	−6.1±0.4	14	150
102.0	1.17± 0.06	99.67±0.02	−11.7±0.5	14	150
109.1	1.40± 0.08	98.98±0.02	44.8±0.3	14	300
116.6	1.27± 0.05	102.90±0.02	−48.2±0.4	14	150
131.0	1.35± 0.09	98.00±0.03	6.6±0.5	14	150
145.6	1.76± 0.17	101.35±0.02	18.2±0.3	14	300
182.1	1.63± 0.14	98.42±0.02	2.8±0.2	14	300
182.1	1.49± 0.08	98.82±0.02	1.9±0.3	18	250
218.4	1.98± 0.15	99.17±0.01	8.5±0.4	18	250
218.4	2.12± 0.19	99.69±0.01	12.7±0.3	14	300
254.6	2.75± 0.32	99.16±0.02	49.5±0.3	18	250
291.1	2.48± 0.15	100.13±0.02	29.1±0.3	18	250
291.1	2.23± 0.18	99.62±0.01	33.3±0.3	14	300

Table 5: Here the results of unordered ice cells equilibrated to 100K and 0.1MPa are shown. "gap" describes the break between switching events. Only simulations that could be identified as reaching a steady state were considered.

uncertainties of the pressure and the overall temperature are the standard error of the mean given by dividing their standard deviation by the square root of the number of data points. The pressure undergoes major fluctuations during one simulation run. Since the thermal conductivity of ice is not strongly pressure dependent, as for example found in [4], no significant deviations are caused by that.

The other parameters of the runs are given in the appendix in section A.1.1. The length of the runs, the starting point of the steady state and the temperature differences between the hot and the cold region are shown in the tables 17, 18 and 19.

The plots of the thermal conductivity values for the different temperatures and cells are shown in figures 7, 8 and 9. As described in section 3.4 plotting the resistivity against l_z^{-1} allows to extrapolate the bulk thermal resistance as the y axis intercept. Therefore, here plots of $\kappa^{-1}(l_z^{-1})$ are shown.

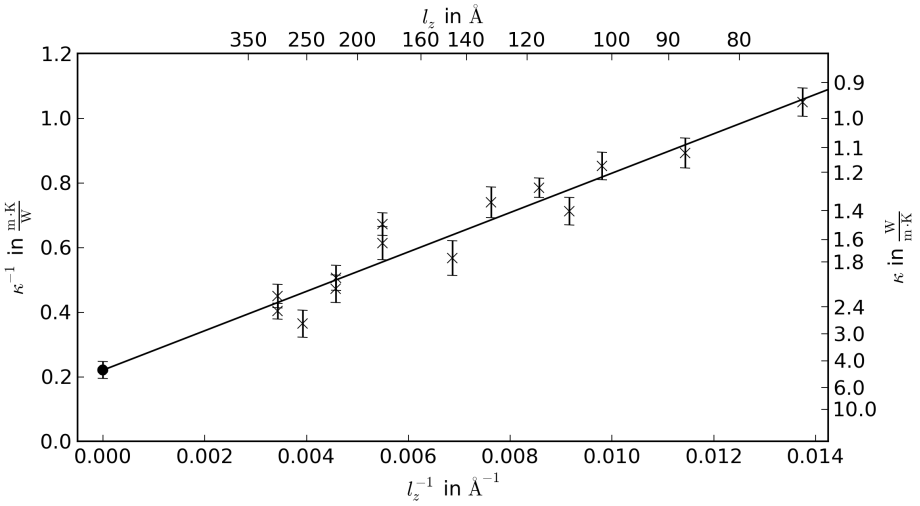

Figure 7: The results for all converged unordered cells at 100K along the c direction are shown. The y axis intercept corresponds to the extrapolated bulk value.

Unordered Cells at 150K along c:			
l_z [Å]	κ [W/m/K]	$\bar{T}$ [K]	$\bar{p}$ [MPa]
102.0	1.05±0.05	148.27±0.03	72.3±0.4
124.1	1.23±0.05	147.37±0.02	−6.9±0.3
145.9	1.35±0.02	152.09±0.02	9.1±0.4
182.3	1.66±0.12	152.66±0.02	23.8±0.4
219.1	1.65±0.09	148.57±0.02	−27.9±0.3

Table 6: Here the results of unordered ice cells equilibrated to 150K and 0.1MPa are shown. All runs were done with 14 strips and with a gap of 300fs between switchings. One run was omitted because of lack of convergence.

The linear relationship is clearly visible in cases of 100 and 200K. The solid lines correspond to the extrapolation fit, which is found as described in section 3.6.2. The fit shows a decent agreement for all temperatures. In the case of 100 and 200K the large amount of data points allows a more precise fit. In the case of 150K the slope of the fit differs from the other two. It also

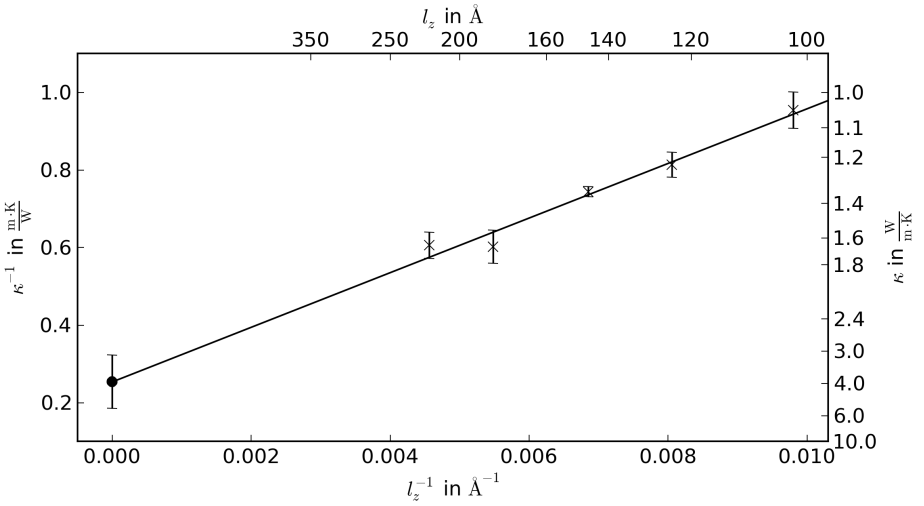

Figure 8: The results for all converged unordered cells at 150K along the c direction are shown. The y axis intercept corresponds to the extrapolated bulk value.

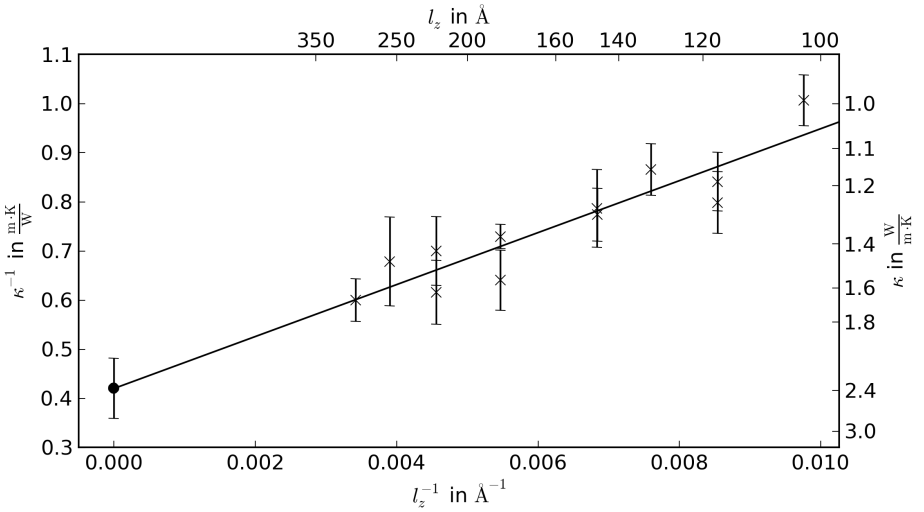

Figure 9: The results for all converged unordered cells at 200K along the c direction are shown. The y axis intercept corresponds to the extrapolated bulk value.

Unordered Cells at 200K along c:					
l_z [Å]	κ [W/m/K]	$\bar{T}$ [K]	$\bar{p}$ [MPa]	n_{str}	gap [fs]
102.5	0.99± 0.05	199.26±0.05	−10.7±0.7	14	150
117.1	1.19± 0.08	201.84±0.05	1.6±0.7	14	150
117.1	1.25± 0.10	202.70±0.04	−0.6±0.6	18	250
131.6	1.16± 0.07	198.31±0.05	26.2±0.7	14	125
146.3	1.27± 0.13	196.40±0.05	11.5±0.9	14	125
146.2	1.29± 0.09	202.23±0.03	27.8±0.4	14	300
182.9	1.56± 0.15	197.76±0.03	1.6±0.5	18	250
182.9	1.37± 0.05	197.73±0.03	2.4±0.4	14	300
219.3	1.43± 0.14	201.43±0.03	42.7±0.5	18	250
219.3	1.62± 0.17	200.47±0.03	40.8±0.4	14	300
256.1	1.47± 0.20	197.82±0.03	−5.1±0.5	18	250
292.4	1.67± 0.12	198.92±0.03	29.3±0.6	14	300

Table 7: This table shows the results of unordered ice cells equilibrated to 200K and 0.1MPa. "gap" describes the break between switching events. Again only simulations that could be identified as reaching a steady state were considered.

T[K]	$\kappa_{\mathrm{bulk}}^{-1}$[m·K/W]	m[m^2 · K/W]	κ_{bulk}[W/m/K]	κ_{exp}[W/m/K]
100	0.220 86±0.026 50	60.9± 3.6	4.53±0.54	6.50±0.33
150	0.253 57±0.068 96	70.4±10.0	3.94±1.07	4.30±0.21
200	0.420 16±0.061 11	52.9± 9.0	2.38±0.35	3.15±0.16

Table 8: The fit parameters found in the extrapolation of the bulk thermal conductivity for proton disordered cells are shown. m is the slope of the extrapolation plot. The experimental values are computed from the parametrization in equation (8) taken from [3].

shows a large uncertainty. Additional data points would be needed to allow a more exact extrapolation.

The extrapolated bulk thermal conductivities are listed in table 8. The corresponding experimental values are computed from the parameterizations in equation (8) taken from [3] as described in section 2.2.2.

Especially for lower temperatures the experimental values are significantly

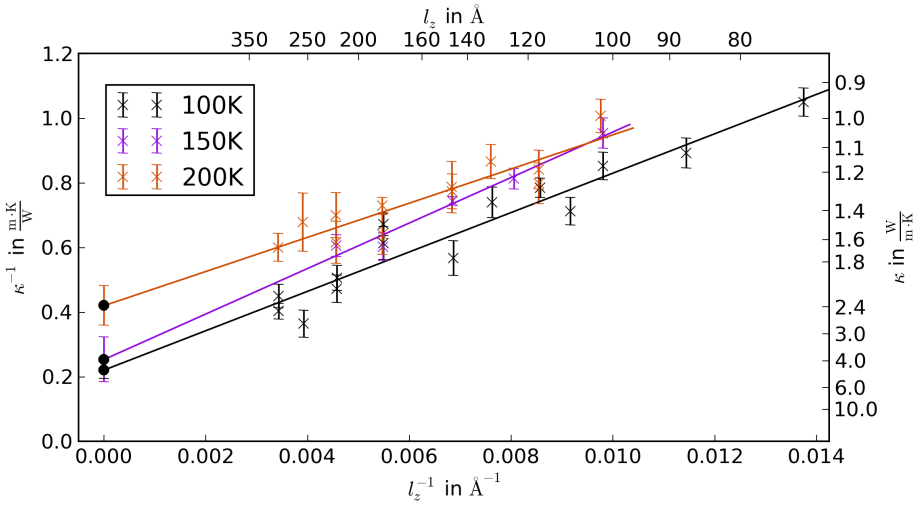

Figure 10: In this plot the results for unordered cells at 100, 150 and 200K are shown.

higher than the values found in this work. This is not unexpected. Earlier studies, for example by English et al. [11] on ice Ih using the TIP4Pice model, also found lower thermal conductivities than experimentally expected.

As expected the thermal conductivity decreases for increasing temperatures. This can be seen very well in the comparison of the different cell lengths for the three temperatures. This is plotted in figure 10. The values for 150K lie between the points for 100 and 200K. This is visible even considering the large uncertainties of the individual values. The same behavior is seen in the extrapolated values. Due to the large uncertainty in the extrapolation of the 150K data this is not significant for the bulk value, but in the individual data points the trend is clearly visible.

Also the slopes of the three extrapolation curves are very similar. According to the rough derivation in [28] the slope of the extrapolation is dependent on the heat capacity of the branches significantly contributing to the heat current and the sound velocity of the crystal. Those quantities will not differ strongly for the three temperatures considered here. The agreement of the three slopes is therefore expected. The slope of the extrapolation for 150K is relatively large compared to the other two values. This is another indicator that more data points are needed for that temperature to allow a decent extrapolation. A more precise analysis of the slopes is given in section 4.5.

Unordered Cells at 100K along a/b:			
l_z [Å]	κ [W/m/K]	$\bar{T}$ [K]	$\bar{p}$ [MPa]
89.5	1.67±0.11	99.51±0.02	36.9±0.5
134.2	2.08±0.11	100.03±0.01	58.3±0.4
178.7	1.66±0.10	99.73±0.01	114.4±0.3
223.5	2.22±0.19	101.69±0.01	84.7±0.3
268.3	2.66±0.13	100.51±0.01	77.5±0.3

Table 9: The results along the a/b direction for cells equilibrated to 100K and 0.1MPa are listed. All runs use a 600 step gap between switches and 14 strips.

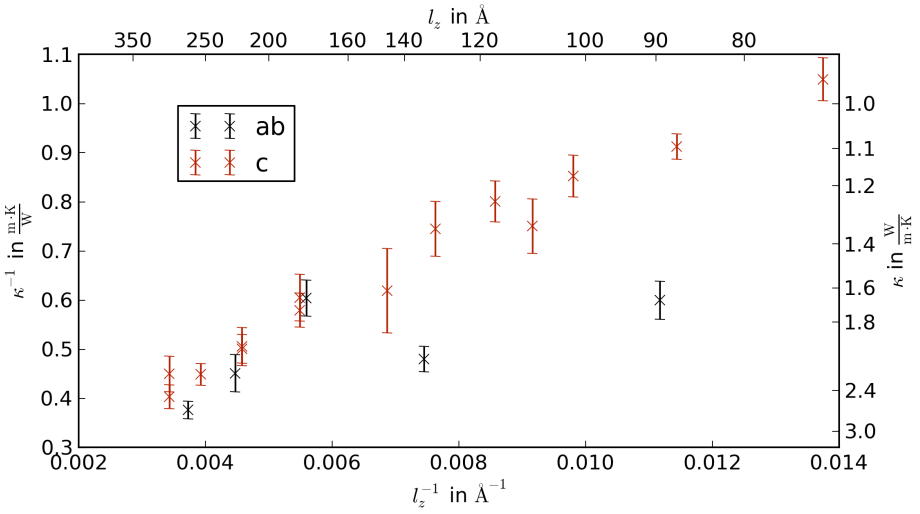

Figure 11: In this plot the examined unordered cells at 100K are shown for both the a/b and the c direction. The runs for the a/b direction do not give a consistent picture. The smaller two cells deviate significantly from the c direction results. The largest cell also seems to have a thermal conductivity being too high. The other values agree well.

To verify the low anisotropy of the thermal conductivity in ice Ih, also cells with a heat flux along the a/b direction are being simulated. The cells use a similar geometry as for the runs along the c direction. The cell is turned so that one of the a/b axes is aligned with the z axis of the cell. The

cross-sectional area is set to three unit cells in the other a/b direction and two unit cells along the c direction.

Only one temperature is examined. All anisotropy effects should be visible for 100K. The results for the different cell lengths are then compared to the results for the c direction. The results are shown in table 9. As for the other runs the additional parameters are shown in the section A.1.1 in table 20.

A comparison of the two crystal directions is shown in figure 11. It is obvious that the two values for the smaller cells along the a/b direction do not agree with the c direction. This cannot be explained by the presence of large fluctuations. Also the thermal resistivity of the longest cell is significantly lower than the corresponding values along the c direction. A possible explanation for this behavior is that the examined cells only have two unit cells along the c direction. Possibly even with an overall dipole moment of near zero there can be two partially ordered sections canceling each others dipole moment. But overall the deviations are not well understood.

The other two values agree well with the c direction. Generally more runs with larger cross-sectional areas are needed to find the true anisotropy in the system. Nonetheless, the results for the c direction are believed to represent the effects of temperature changes and proton ordering well. So the results still give a good representation of the systems under examination.

4.3 Ordered Ice XI

Ordered cells are simulated at temperatures of 100 and 200K. Because of the low resolution of the method, there are no values for 150K taken into account. As for the unordered case, first the values for temperature gradients along the c direction are shown.

The results for all decently converged cells at 100 and 200K are shown in tables 10 and 11 respectively. Especially in the ordered case all runs for cells shorter than $\approx$100Å do not show a decent steady state. Therefore, all those runs are excluded. This is ascribed to the fact that for ordered ice, the mean free path is longer than for ice Ih. It can be seen already from the experimental results that the thermal conductivity is much larger for the proton ordered than for the proton disordered phase. For those long mean free paths, the ballistic heat transport still dominates for larger separations of the reservoirs.

Nonetheless, the same time constraints as for the unordered cells apply. Therefore, it is not feasible to simulate cells with an even larger separation

Ordered Cells at 100K along c:			
l_z [Å]	κ [W/m/K]	$\bar{T}$ [K]	$\bar{p}$ [MPa]
116.5	2.45± 0.47	101.71±0.02	0.4± 0.3
131.1	2.82± 0.08	101.95±0.02	10.1± 0.3
145.7	3.36± 0.55	102.36±0.02	−15.2± 0.3
182.1	3.79± 0.79	100.79±0.01	−12.4± 0.3
218.5	3.49± 0.20	101.37±0.01	7.3± 0.3
291.3	4.60± 0.44	100.19±0.01	2.3± 0.2

Table 10: Here the results of ordered ice cells equilibrated to 100K and 0.1MPa are listed. All runs are done using 14 strips and a 375fs separation between heat transfers. Shorter cells were simulated but failed to converge due to the long mean free path.

between the reservoirs. As for the unordered case, the longest cell lengths are ≈300Å. Also only runs with a relatively low heat current are available. One possible improvement could be the inclusion of additional data points with higher heat currents. This has not been done because of the higher risk of non-physical waves or drifts and the risk of leaving the linear response regime for high heat currents.

The other parameters of all runs are shown in the tables 21 and 22 in the section A.1.2 in the appendix.

The extrapolation plots corresponding to the given values are shown in figures 12 and 13. Again the values are plotted in an κ^{-1} against l_z^{-1} plot to allow the linear extrapolation fit. The data points again agree relatively well with the linear fit. The agreement is much better in the case of 100K. For 200K the values vary more, which is ascribed to the much larger thermal fluctuations.

Generally the uncertainties of the extrapolated bulk thermal conductivities are much larger in the ordered case. The fit parameters of the extrapolation are shown in table 12. The absolute uncertainties for the extrapolated thermal resistivity differ for both cell types and most temperatures by a maximum of a factor of two. The ordered cells have a larger uncertainty because of the smaller amount of runs that are available.

Nonetheless, the main factor for the large uncertainties in the thermal conductivity is the fact that for the same absolute uncertainty in the thermal

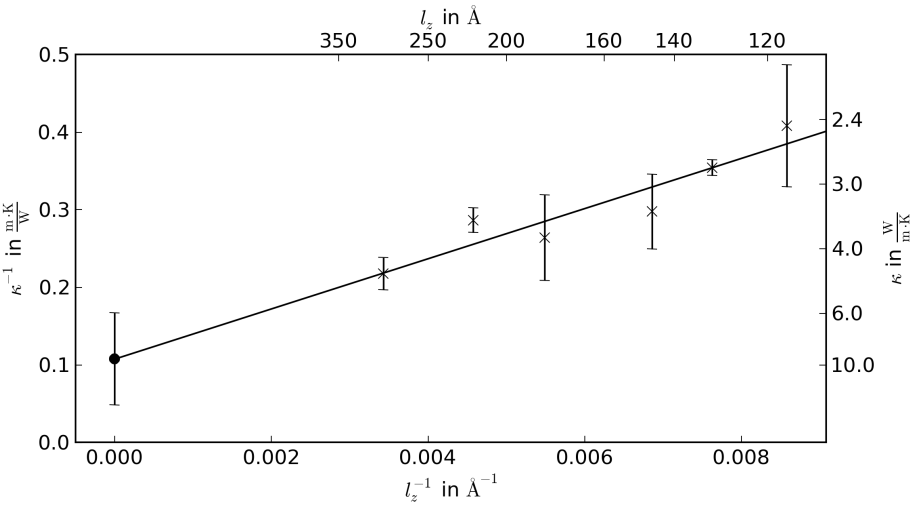

Figure 12: The results for all converged ordered cells at 100K along the c direction are shown. The y axis intercept corresponds to the extrapolated bulk value.

Ordered Cells at 200K along c:			
l_z [Å]	κ [W/m/K]	$\bar{T}$ [K]	$\bar{p}$ [MPa]
117.4	1.54± 0.09	198.56±0.03	−107.7± 0.5
131.8	1.92± 0.14	202.63±0.03	−37.0± 0.4
146.5	2.04± 0.06	197.79±0.03	−52.0± 0.5
183.1	1.72± 0.09	201.90±0.03	−33.2± 0.4
256.2	2.27± 0.18	201.06±0.03	−13.2± 0.4
292.5	2.78± 0.29	200.93±0.03	13.4± 0.4

Table 11: The results of ordered ice cells equilibrated to 200K and 0.1MPa are shown. All runs are done using 14 strips and a 375fs separation between heat transfers. Again some runs are excluded because of lack of decent convergence.

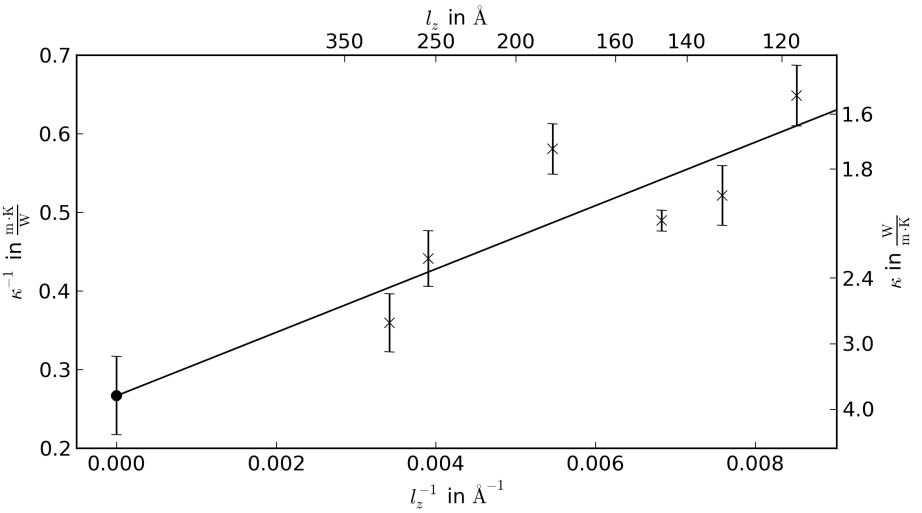

Figure 13: The results for all converged ordered cells at 200K along the c direction are shown. The y axis intercept corresponds to the extrapolated bulk value.

T[K]	$\kappa_{\mathrm{bulk}}^{-1}$[m·K/W]	m[m^2 · K/W]	κ_{bulk}[W/m/K]	κ_{exp}[W/m/K]
100	0.107 46±0.059 33	32.3±11.3	9.31±5.14	6.50±0.33
200	0.267 10±0.049 67	40.3± 8.0	3.74±0.70	4.00±0.24

Table 12: The fit parameters found in the extrapolation of the bulk thermal conductivity for proton ordered cells are shown. m is the slope of the extrapolation plot. As explained in the text, the uncertainty of the extrapolated thermal conductivity for 100K is questionable because of the large relative uncertainty in the found thermal resistivity. The experimental values are computed from the parametrization in equation (8) taken from [3].

resistivity, the relative uncertainty will be much larger for the smaller thermal resistivity in the ordered case. Especially for the ordered cell at 100K the relative uncertainty becomes 55%. Here the probability distribution of the thermal conductivity will not be approximated well as symmetric anymore.

To get a rough approximation of the uncertainty of the extrapolated value the upper and lower bounds are estimated by inverting $\kappa_{\mathrm{bulk}}^{-1} + \Delta(\kappa_{\mathrm{bulk}}^{-1})$ and

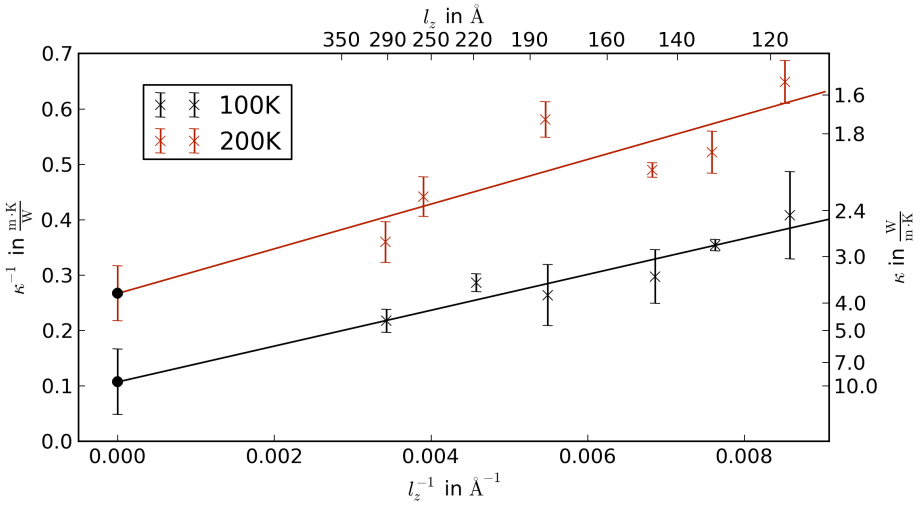

Figure 14: In this plot the results for ordered cells at 100 and 200K are shown.

$\kappa_{\mathrm{bulk}}^{-1} - \Delta(\kappa_{\mathrm{bulk}}^{-1})$ separately. As mentioned before, this will just give a rough approximation of the uncertainty, but for a more careful analysis, the probability distributions would have to be known. Since all interesting results can already be seen in the extrapolated thermal resistivity and the comparison of the values for different cell lengths, no further effort is made to find the true distribution for the thermal conductivity in this case.

The upper and lower bound that are found are $\kappa_{\mathrm{bulk,lower}} = 6.00\frac{\mathrm{W}}{\mathrm{m\cdot K}}$ and $\kappa_{\mathrm{bulk,upper}} = 20.78\frac{\mathrm{W}}{\mathrm{m\cdot K}}$. The estimated value for the bulk thermal conductivity is $9.31\frac{\mathrm{W}}{\mathrm{m\cdot K}}$. Obviously the uncertainty interval is not symmetric for a relative uncertainty of this size. Considering the rough estimation of the interval above, the significant deviation from the extrapolated thermal conductivity of unordered ice at 100K becomes much more pronounced. A further comparison of the two cell types is given in the next section.

Again the temperature dependence of the thermal conductivity is qualitatively well represented. Even for the bulk thermal conductivity which is subject to large uncertainties, the thermal conductivity for 100K is significantly higher than for 200K. The same difference can be seen well for the different cell lengths as well. This is shown in figure 14.

Also the slope of the extrapolation fit is similar for both temperatures. As explained for the unordered case this supports the validity of the fit. The

specific heat and the sound velocity of the ordered crystal should not differ largely between 100 and 200K. Therefore, the slope of the curves should not differ much as well.

Ordered Cells at 100K along a/b:			
l_z [Å]	κ [W/m/K]	$\bar{T}$ [K]	$\bar{p}$ [MPa]
111.8	2.29±0.09	100.85±0.02	−0.3±0.5
134.2	1.95±0.20	100.27±0.02	−2.7±0.4
178.8	3.61±0.32	100.50±0.01	27.4±0.3
223.8	3.20±0.26	100.20±0.01	−15.2±0.3
268.3	5.07±1.15	100.31±0.01	14.2±0.4

Table 13: The results along the a/b direction for proton ordered cells equilibrated to 100K and 0.1MPa are listed.

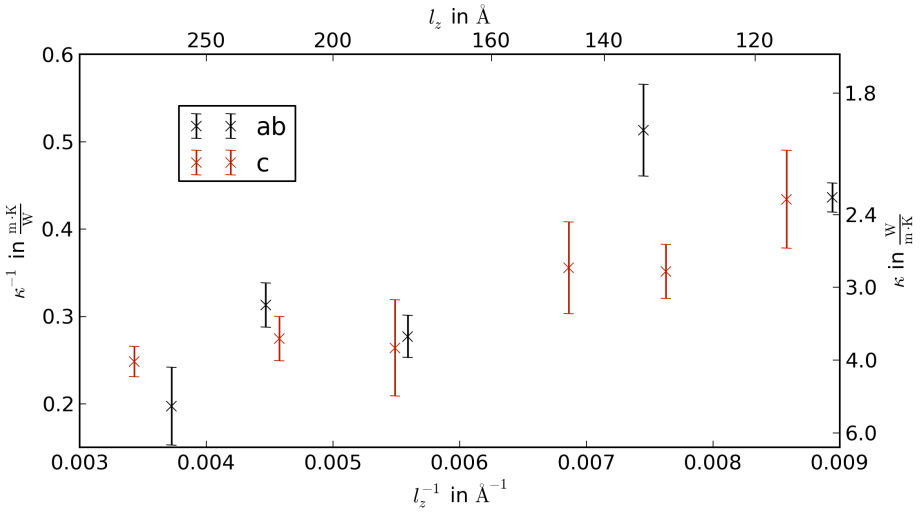

Figure 15: The results for both crystal directions in ordered cells at 100K are shown. There are no significant deviations between the directions. Therefore, it is sufficient to only examine the c direction.

To verify that the anisotropy of the ordered ice cells is negligible, also cells with a heat flux along the a/b direction of the crystal are shown. Only cells at 100K are examined. The results are listed in table 13. As always,

the other parameters of the simulation runs can be found in the appendix. They are given in table 23.

Plotting the values together with the values for the c direction does show deviations but no significant trend can be seen. The plot is shown in figure 15. The deviations are purely statistical and do not show a significantly different trend from the c direction results.

Therefore, the direction of the heat current does not have a significant influence. Because of that, the examination of cells only along the c direction will give a significant understanding of the underlying physics.

4.4 Comparison

In the previous two sections the results for the simulated ordered and disordered structures at different temperatures have been presented. The extrapolated bulk thermal conductivities are plotted together with the parameterizations from [3] shown in equation (8) in figure 16.

As described in the previous, section the uncertainty of the bulk thermal conductivity of proton ordered ice at 100K cannot be estimated very well because of the lack of knowledge of its distribution. Therefore, in the plot, both proposed intervals are shown. The blue interval is found by uncertainty propagation, ignoring the lack of linearity. The second interval is found by the alternative method of inverting the upper and lower bound of the uncertainty in the thermal resistivity as described in the previous section. It is shown as a thick black interval.

Both intervals are very large. The blue interval is overestimating the lower and underestimating the upper uncertainty. This is due to the assumption of symmetry of the interval which is not valid in this case. The black interval is believed to give a still rough but better justified estimate of the uncertainty.

Comparing the results to experiment, especially at lower temperatures, the simulations seem to show a thermal conductivity which is significantly too low. The value for 150K is very inexact. Additionally, the slope of the extrapolation curve is much larger than for the other two extrapolations in the unordered case. Under the assumption that this is caused by the insufficient number of data points, this leads to an overestimation of the thermal conductivity. Therefore, the visible but not significant twist of the inverse temperature dependence is believed to be due to fluctuations and insufficiency of data rather than being an actual property of the method or the model.

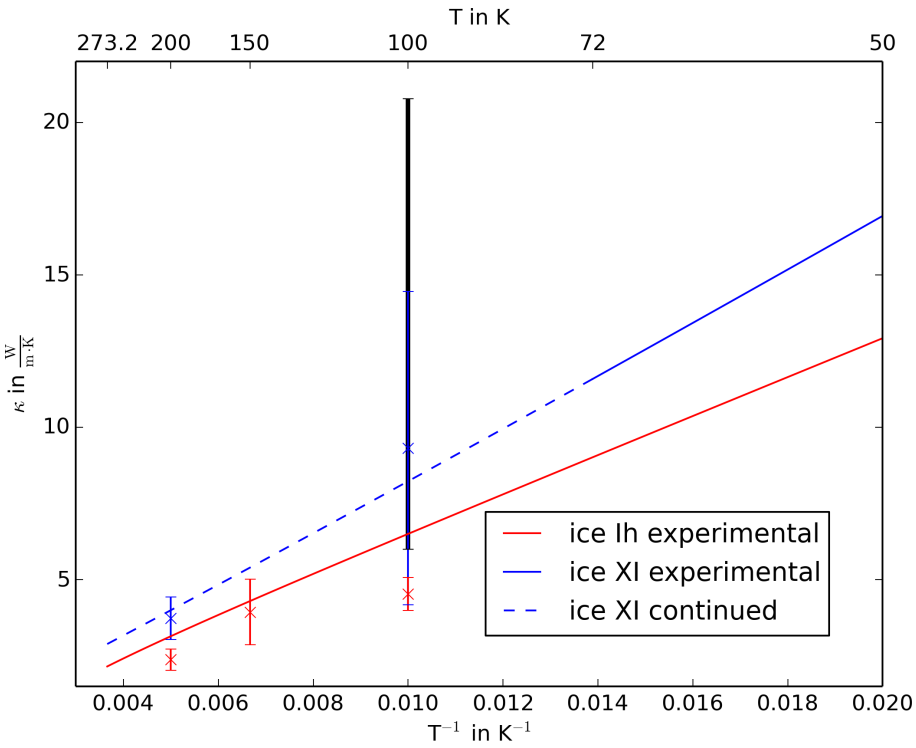

Figure 16: In this plot the extrapolated results for the proton ordered and disordered cells are compared to the parameterizations taken from [3] and given in equation 8. The values differ significantly as already described in the previous sections. Nonetheless, the overall trends are described qualitatively.

The underestimation of the thermal conductivity cannot be explained by uncertainties of the method and is therefore ascribed to the properties of the model. Apparently the TIP4P/2005f model does not correctly reproduce the thermal conductivity of ice Ih. Using the TIP4PIce model, which is optimized for the solid phases of H_2O, English et al. [11] measured the thermal conductivity of ice Ih by using a Green-Kubo-based method. They found even lower values for the thermal conductivity. It seems that the TIP4P models generally underestimate the thermal conductivity of ice Ih.

Even though the direct comparison with the experimental values does not give satisfying results, the general mechanisms seem to be reproduced decently well. As mentioned above, both cell types show the expected in-

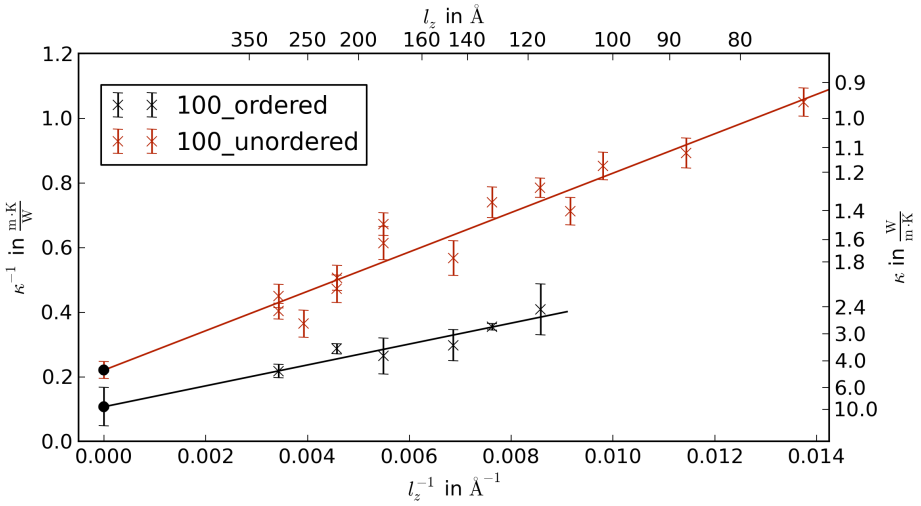

Figure 17: A comparison of all data points for ordered and unordered ice at 100K is shown.

crease in thermal conductivity for lower temperatures. Additional data points would be needed to quantify the exact temperature dependence. Nonetheless, the overall trend seems to be decently reproduced.

The main goal of this work was to examine the influence of the proton ordering on the thermal conductivity of ice. This influence is reproduced well already in the extrapolated bulk values. Even considering the large uncertainties, the thermal conductivity at a certain temperature is always significantly higher for the proton-ordered ice. Also the gap shrinks for higher temperatures as seen in figure 16. The large uncertainties do not allow a more careful analysis of the separation though.

Comparing the runs for different cell lengths at one temperature, the difference can be seen very well. Plots for this comparison are given in figures 17 and 18 for 100 and 200K respectively. The separation of the two cell types is obvious in both cases. As expected, the gap between the values is larger for 100K, but even for the strongly fluctuating values at 200K and the expected smaller differences, the separation is still significant.

The slope of the extrapolation differs for the two cell types as well. The slope for the proton-ordered cells is significantly lower than for the proton-unordered structures. This is discussed in more detail in the next section.

It can be concluded that even though the model and the extrapolation

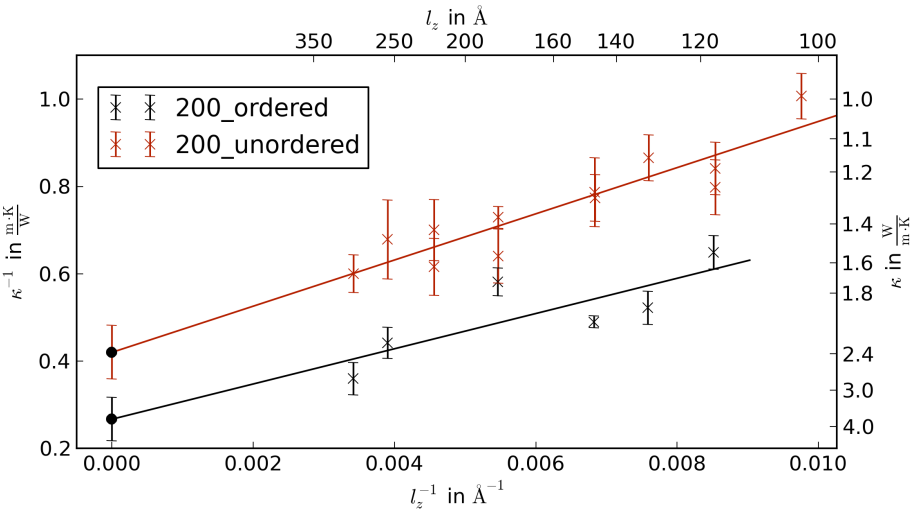

Figure 18: This plot compares the ordered and unordered ice cells at 200K.

method are not able to reproduce the experimental thermal conductivity, the differences between the ordered and unordered cells, as well as the temperature dependence for the thermal conductivity in one cell type, are reproduced qualitatively.

4.5 Sound Velocity

In their simple Debye model derivation, Schelling et al. [28] derived the slope of the extrapolation to be $12/(c_v v)$. Here c_v is the specific heat of the phonon modes contributing significantly to the heat current. They assume that these are the acoustic modes. v is the average sound velocity. This prediction is rather rough and can therefore just give a qualitative understanding of the main influences on the slope. This is the purpose of the present section.

The specific heat of the acoustic modes is assumed to be given by the Dulong-Petit limit as in [28]. Therefore, it should not differ for the proton ordered and unordered structures. Under the assumption that their derivation is correct and the specific heat is actually the same, the sound velocities of the two crystals should differ to explain the deviations of the extrapolation slope.

The sound velocities are given by the slopes of the acoustic branches of the phonon dispersion near the Γ point. The phonon dispersion relations of

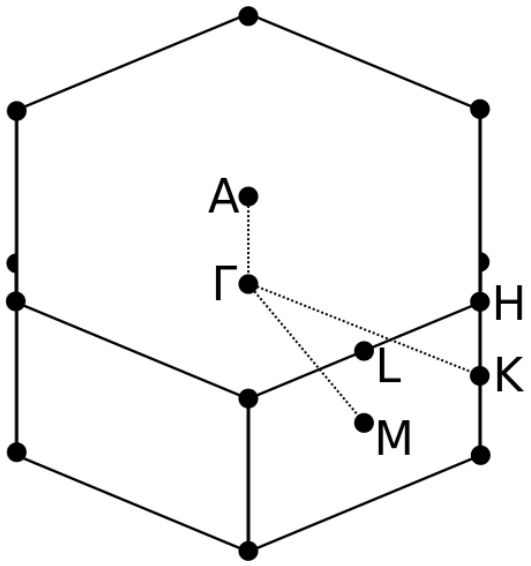

Figure 19: Here the first Brillouin zone is shown with the high symmetry points used in the phonon dispersion graphs.

ice Ih have been found experimentally by Dorner [10] by inelastic neutron scattering. For ice XI, due to the impossibility to produce a pure sample, there are only results for ab initio lattice dynamics calculations, for example by Wehinger, Chernyshov, Krisch, Bulat, Ezhov, and Bosak [33]. Their results are shown in figures 20a and 20b respectively. The plots are taken directly from their papers. Only a change of the axes labeling is done.

The rough estimates of the sound velocities found by doing a manual fit to their plots are given in table 14. They seem to be significantly higher for ice XI. This is a possible explanation for the reduced slope in the ordered cells. The differences seem to be not high enough to account for the rather drastic change. But the general direction is given correctly.

The generally lower sound velocity of the transverse branches along the $c*$ direction (ΓA) seems to suggest that the system is more anisotropic than expected. Nonetheless, for the thermal conductivity the longitudinal branch is dominant. It does not seem to show a significant difference between the directions. This is a possible explanation for the lack of anisotropy found in experiment.

To check if these values are reproduced by the TIP4P/2005f model one has to get the phonon dispersion relations for ice Ih and ice XI from simulations

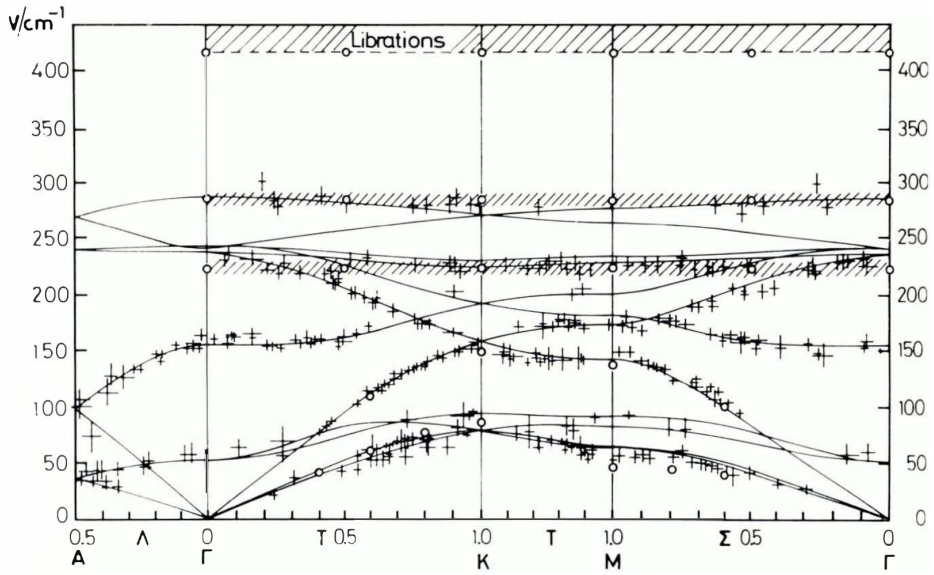

(a) ice Ih

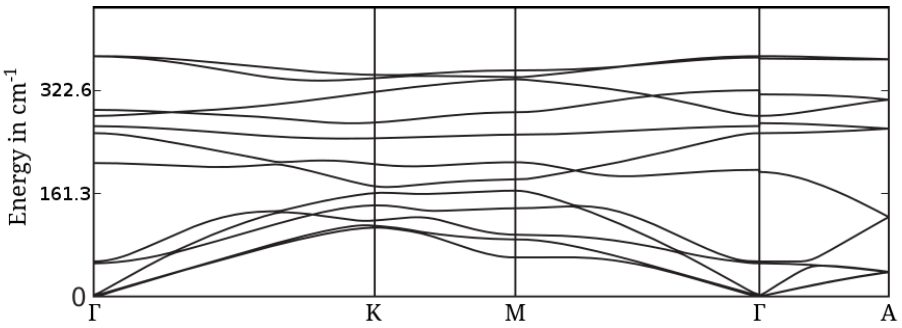

(b) ice XI

Figure 20: The experimental phonon dispersion curve for ice Ih found by and taken from Dorner [10] is shown in (a). The plot of the phonon dispersion curve for ice XI found by ab initio lattice dynamics calculations by Wehinger et al. [33] and taken from this paper, is shown in (b).

ice	direction	v_T[km/s]	v_L[km/s]
Ih	ΓA	1.6±0.3	4.3± 0.3
Ih	ΓK	2.5±0.4	4.4± 0.3
Ih	ΓM	2.3±0.4	4.5± 0.3
XI	ΓA	1.8±0.4	5.5± 0.4
XI	ΓK	2.8±0.4	5.4± 0.4
XI	ΓM	2.9±0.4	5.6± 0.4

Table 14: In this table the sound velocities estimated from the slopes of the phonon dispersion curves of ice Ih from [10] and ice XI from [33] shown in figure 20 are listed. The values for ice XI seem to be higher especially for the longitudinal velocities.

as well.

This is tried using scripts provided by Marivi Fernandez-Serra as well as the arce package [24] and the vibrator program of the siesta package [30]. For the ordered ice, a four molecule unit cell is repeated to obtain a three by three by three super-cell. For the unordered ice the same procedure is done using a 32 molecule unit cell to be able to capture the effects of the disordered protons. The crystal is first annealed by cooling it in 1K steps from 5K to 1K. The arce package and the NPT ensemble are being used. Then an additional longer run is done at 0.5K to obtain an estimate of the relaxed structure.

Using a script written by Marivi Fernandez-Serra, the force constant matrix is computed by moving the atoms in the central cell and then computing the resulting force by use of a modified arce package [24]. This is then used as input for the vibrator program. The lower bands of the resulting phonon dispersion curves are shown in figures 21 and 22.

The negative regions directly show that the structure is not fully relaxed yet. This also can be seen by checking the force constants matrix. The fact that there are significantly negative values found shows that additional effort would be needed to find the actual relaxed structure. The reason for this is probably the lack of anisotropic cell size fluctuations during the annealing. Nonetheless, there are already well represented branches seen. Their sound velocities are compared to the experimental results. The considered branches are marked by thick black lines. In the case of the ice Ih only half the Brillouin zone is shown because of the doubled size of the unit cell examined.

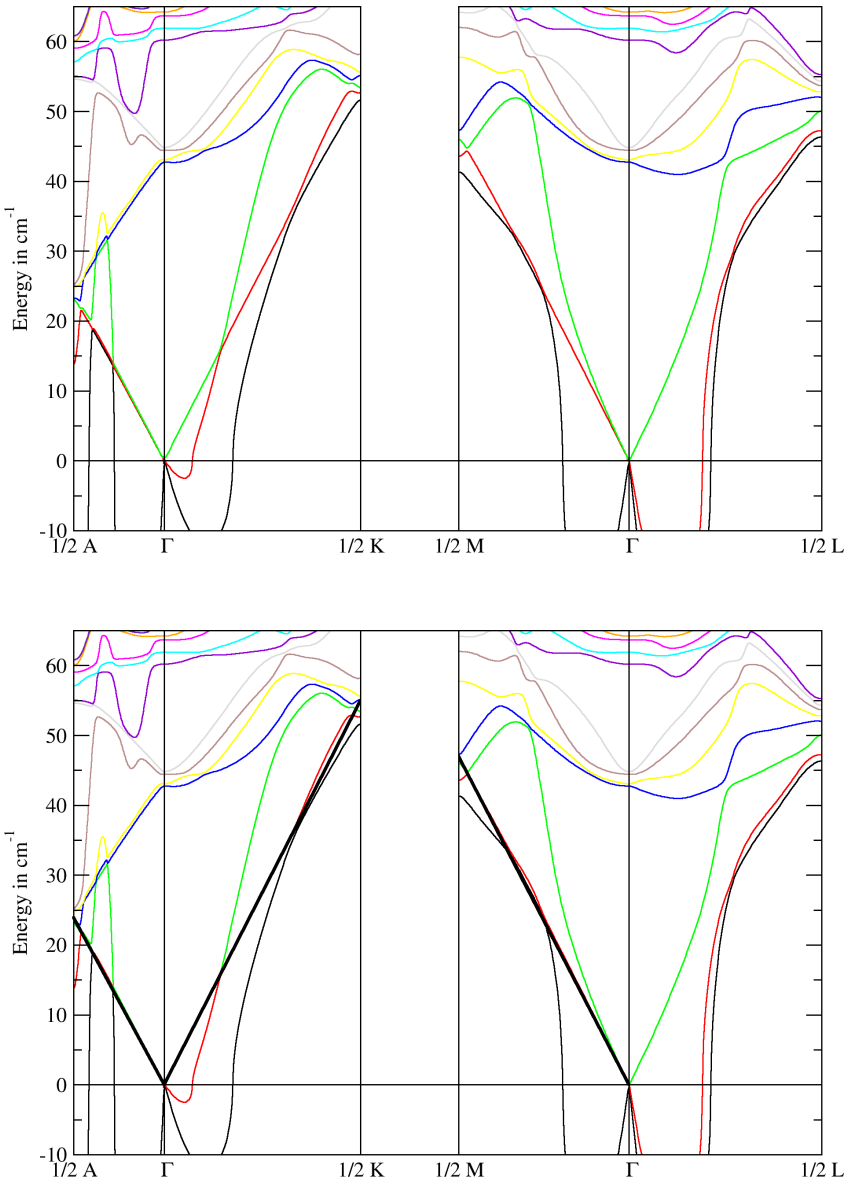

Figure 21: Here the phonon dispersion relations for a 32 molecule unit cell found by the vibrator program of the siesta package [30] are shown. To see the influence of the proton disorder not the four molecules unit cell but a 32 molecule structure is used. Therefore, the displayed regions show only half the Brillouin zone of the four molecule cell for each direction. The black lines are drawn to estimate the slope of the acoustic branch and therefore the sound velocity.

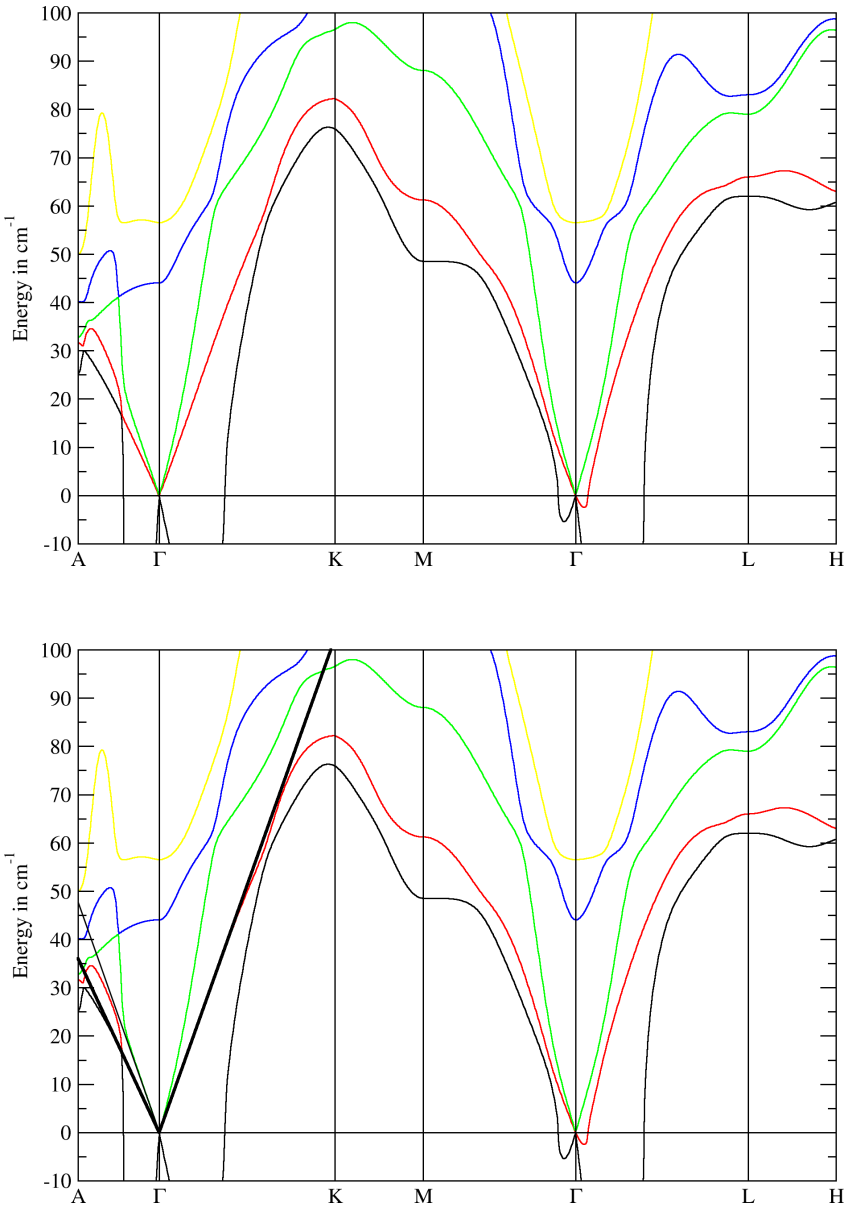

Figure 22: Here the phonon dispersion relations for one unit cell of ice XI found by the vibrator program of the siesta package [30] are shown. The black lines are drawn to estimate the slope of the acoustic branch and therefore the sound velocity.

ice	direction	v[km/s]
Ih	ΓA	2.1
Ih	ΓK	2.5
Ih	ΓM	2.5
XI	ΓA	1.6/2.1
XI	ΓK	2.4

Table 15: Here the sound velocities found by the vibrator program [30] are shown. It is not possible to give a decent uncertainty since the phonon dispersion curves show behavior of unrelaxed cells and therefore the curves themselves are of questionable accuracy. The values are of the order of the transverse sound velocities found in table 14. There are two values for ice XI in the ΓA direction since there are two distinct lines. Nonetheless, they both seem to correspond to the transverse branches.

The resulting sound velocities are shown in table 15. Except for ice XI along the c direction there always is one or no decently linear acoustic branch. The other branches are not shown correctly due to the non-relaxed structure. In the case of ice XI along the c direction the slopes of the two different branches are so close to each other that they are believed to both correspond to the transverse branch which should be degenerate. Generally all shown branches show sound velocities which correspond roughly to the reference values. They seem to be too high for the ΓA direction for both cells and too low for the ΓK direction of ice XI. A more careful comparison to the experimental values would require the actual relaxed structure.

4.6 Defects

Finally it is checked whether the method can reproduce the expected reduction in thermal conductivity due to defects in the structure. This is done introducing two different types of point defects. First two HOD molecules are introduced by changing the mass of one of the hydrogens in a molecule to the deuterium mass of 2.014102u. The point defects are introduced at the two centers between the reservoirs. The resulting change in thermal conductivity is expected to be rather small. Therefore, an additional run is performed using a more severe non-physical defect. The oxygen in two molecules is replaced by an atom X which has a non-physically high mass of 1000u. The

	l_z [Å]	κ [W/m/K]	$\bar{T}$ [K]	$\bar{p}$ [MPa]
pure	218.5	3.49±0.20	101.37±0.01	7.8±0.2
HOD	218.4	3.63±0.20	101.89±0.01	18.8±0.3
H_2X	218.5	3.02±0.26	99.95±0.01	11.4±0.2

Table 16: The results of the two different point defect types are shown together with the corresponding pure structure. The defect runs are using a 600 steps gap and 14 strips. The switching was run for 400ps and the steady state was determined to start after 250 and 225ps for HOD and H_2X respectively.

defects are positioned in the same spot as the HOD in the other run. For both runs proton-ordered structures are used.

The cells are first equilibrated to 100K and 0.1MPa and then examined using the same procedure as for the pure cells. The results and the corresponding value for the pure cell taken from table 10 are shown in table 16. Also the three values are plotted in figure 23.

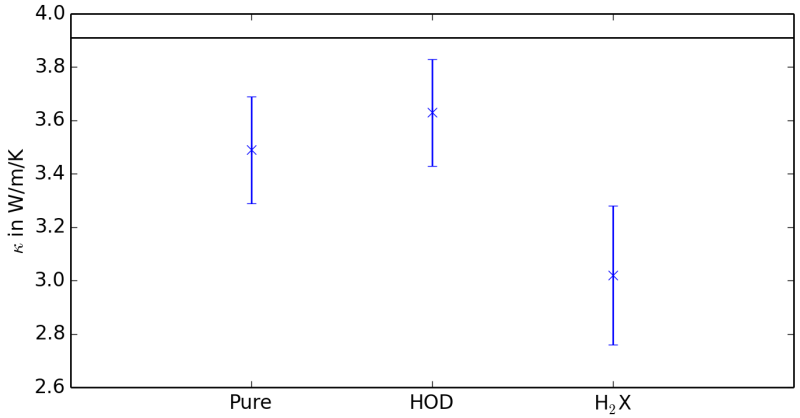

Figure 23: Here the thermal conductivity values for ordered cells of the same size with and without defects are shown. Additionally, the value of the extrapolation curve at the corresponding length is shown as a black line.

There is no significant difference seen for the pure and the HOD defect

cell. The HOD defect cell even seems to lie a little over the pure cell but the difference is not significant. Comparing it to the value found by the extrapolation fit of 3.91W/m/K shows that it is rather lower than the value for the pure cells. This difference is also not statistically significant. This is somewhat expected since the introduced additional mass is rather small and does not severely change the system.

The thermal conductivity for the H_2X defect is significantly smaller than the other two cells. This is expected since the very heavy molecule will basically not vibrate and therefore reduce the thermal flux carried by phonons drastically.

Obviously the resolution of the method is not able to distinguish between pure cells and a rather small defect as an introduced HOD molecule. Larger defects are needed to show a significant deviation.

5 Summary and Outlook

In this work the thermal conductivity of hexagonal ice with ordered and unordered proton structure was examined. This was done by molecular dynamics simulations using the direct method proposed by Müller-Plathe [20]. This non-equilibrium method allows direct computer measurements of the thermal conductivity of the system under examination.

Proton-ordered and unordered structures were examined at multiple cell sizes and temperatures along the c axis of the crystal. Using the Matthiessen's rule approach proposed by Schelling et al. [28], the bulk limit was estimated for proton unordered cells at 100, 150, and 200K, and for ordered cells at 100 and 200K.

The resulting values were subject to large uncertainties. Nonetheless, they showed the expected rise in thermal conductivity for decreasing temperature. This could already be seen very well, comparing the single cells.

Also the comparison of the ordered and unordered cells shows the expected higher thermal conductivity for ordered cells. Furthermore, the experimentally observed increase of this effect for lower temperature can be seen in the results of this work as well.

The phonons that are dominant for the heat transport are the acoustic phonons. If there is no change in the intra-molecular bond length, the proton structure should not have a big influence on the thermal conductivity. The hydrogen bond's strength is strongly dependent on the local electric field. For a rigid model the differences in this local field should be much smaller for different proton configurations. Therefore this result is very promising because it shows that the coupling between the intra-molecular covalent bonds and inter-molecular is sufficiently strong just by using a flexible rather than a rigid model.

Introducing point defects into the cell leads to an expected decrease in thermal conductivity for the more severe of the two defects. Two HOD defects did not show a significant deviation from the pure ice case. The defect seems to be not drastic enough to significantly change the thermal conductivity. Increasing the mass of two oxygens to non-physical 1000u verified that the reduction of the thermal conductivity for severe point defects is reproduced by the method.

To check the validity of the chosen parameters, simulations with cells of different cross-sectional areas or dipole moments were done. It turned out that neither of the two quantities had a significant influence on the thermal

conductivity. Data for the a/b crystal direction gives inconclusive results. For the ordered case no significant deviations from the c axis data is found. The unordered cells showed agreement in some cases but also some significantly deviating values compared to the c axis runs. A more careful analysis is needed to fully understand the reason for this.

The slopes of the extrapolation plots showed a significant difference between the two structures. The proton ordered structures had a lower slope in the $\kappa^{-1}\,(l_z^{-1})$ plot. This can possibly be explained by a larger sound velocity for the ordered structure, which is suggested by the experimental and ab initio lattice dynamics calculation data of Dorner [10] and Wehinger et al. [33]. The attempt to reproduce this by examining the phonon dispersion relations produced by the TIP4P/2005f model failed due to insufficient relaxation of the cells.

Future work on this should include a better determination of the phonon dispersion curve produced by the used water model. Also a more careful analysis could give a better understanding of the finite size effects and the extrapolation method. The inclusion of nuclear quantum effects by the use of path integral molecular dynamics could yield interesting results as well. Since the method seems to generally work well, future work also could address the question of the influence of partial ordering on the thermal conductivity.

The large uncertainties should be addressed in future work as well. Large fluctuations in the heat current and the temperature gradient as well as the lack of very long runs prevent a more quantitative analysis. A possible way of improving the results is for example the implementation of an improved algorithm introducing the heat current. A possible candidate is for example the velocity rescaling algorithm sampling the canonical ensemble, proposed by Bussi, Donadio, and Parrinello [9] and used for a similar work on liquid water by Römer and Bresme [25].

Still the present work has shown that already the rather simple velocity switching algorithm can give decent results. Generally it has been shown that the molecular dynamics simulations using the direct method and the TIP4P/2005f model can qualitatively reproduce the overall behavior of the thermal conductivity of the proton ordered and unordered hexagonal ice. Both the influence of the temperature and of the proton ordering show the correct trend. Future work is necessary to improve the accuracy of the results as well as to fully understand all effects that occurred.

Bibliography

[1] Jmol: an open-source java viewer for chemical structures in 3d. http://www.jmol.org/.

[2] J. L. F. Abascal and C. Vega. A general purpose model for the condensed phases of water: TIP4P/2005. *The Journal of Chemical Physics*, 123 (23):234505, 2005.

[3] O. Andersson and A. Inaba. Thermal conductivity of crystalline and amorphous ices and its implications on amorphization and glassy water. *Physical Chemistry Chemical Physics*, 7:1441–1449, 2005.

[4] O. Andersson and H. Suga. Thermal conductivity of the Ih and XI phases of ice. *Physical Review B*, 50:6583–6588, Sep 1994.

[5] N. W. Ashcroft and D. Mermin. *Introduction to Solid State Physics*. Saunders, Philadelphia, 1976.

[6] D. Bedrov and G. D. Smith. Thermal conductivity of molecular fluids from molecular dynamics simulations: Application of a new imposed-flux method. *The Journal of Chemical Physics*, 113(18):8080–8084, 2000.

[7] J. D. Bernal and R. H. Fowler. A theory of water and ionic solution, with particular reference to hydrogen and hydroxyl ions. *The Journal of Chemical Physics*, 1(8):515–548, 1933.

[8] F. Bresme. Equilibrium and nonequilibrium molecular-dynamics simulations of the central force model of water. *The Journal of Chemical Physics*, 115(16):7564–7574, 2001.

[9] G. Bussi, D. Donadio, and M. Parrinello. Canonical sampling through velocity rescaling. *The Journal of Chemical Physics*, 126(1):014101, 2007.

[10] B. Dorner. Inelastic neutron scattering from ice and other proton-containing substances. *Journal of Glaciology*, 21(85):231–240, 1978.

[11] N. J. English, J. S. Tse, and R. Gallagher. Thermal conductivity in amorphous ices from molecular dynamics. *Physical Review B*, 82:092201, Sep 2010.

[12] M. A. González and J. L. F. Abascal. A flexible model for water based on TIP4P/2005. *The Journal of Chemical Physics*, 135(22):224516, 2011.

[13] O. Haida, T. Matsuo, H. Suga, and S. Seki. Calorimetric study of the glassy state X. enthalpy relaxation at the glass-transition temperature of hexagonal ice. *The Journal of Chemical Thermodynamics*, 6(9):815 – 825, 1974.

[14] T. K. Hirsch and L. Ojamäe. Quantum-chemical and force-field investigations of ice Ih: Computation of proton-ordered structures and prediction of their lattice energies. *The Journal of Physical Chemistry B*, 108(40):15856–15864, 2004.

[15] B. Håkansson and R. G. Ross. Effective thermal conductivity of binary dispersed composites over wide ranges of volume fraction, temperature, and pressure. *Journal of Applied Physics*, 68(7):3285–3292, 1990.

[16] E. Jones, T. Oliphant, P. Peterson, et al. SciPy: Open source scientific tools for Python, 2001. URL `http://www.scipy.org/`.

[17] J. K. Landauer and H. Plumb. *Measurements on anisotropy of thermal conductivity of ice*. Snow Ice and Permafrost Research Establishment, Corps of Engineers, US Army, 1956.

[18] A. J. Leadbetter, R. C. Ward, J. W. Clark, P. A. Tucker, T. Matsuo, and H. Suga. The equilibrium low temperature structure of ice. *The Journal of Chemical Physics*, 82(1):424–428, 1985.

[19] G. J. Martyna, M. E. Tuckerman, D. J. Tobias, and M. L. Klein. Explicit reversible integrators for extended systems dynamics. *Molecular Physics*, 87(5):1117–1157, 1996.

[20] F. Müller-Plathe. A simple nonequilibrium molecular dynamics method for calculating the thermal conductivity. *The Journal of Chemical Physics*, 106(14):6082–6085, 1997.

[21] J. F. Nagle. Lattice statistics of hydrogen bonded crystals. I. the residual entropy of ice. *Journal of Mathematical Physics*, 7(8):1484–1491, 1966.

[22] L. Pauling. The structure and entropy of ice and of other crystals with some randomness of atomic arrangement. *Journal of the American Chemical Society*, 57(12):2680–2684, 1935.

[23] V. Petrenko and R. Whitworth. *Physics of Ice*. Clarendon Press, 1999.

[24] R. Ramirez. arce, 2009.

[25] F. Römer and F. Bresme. Heat conduction and thermomolecular orientation in diatomic fluids: a non-equilibrium molecular dynamics study. *Molecular Simulation*, 38(14-15):1198–1208, 2012.

[26] F. Römer, A. Lervik, and F. Bresme. Nonequilibrium molecular dynamics simulations of the thermal conductivity of water: A systematic investigation of the SPC/E and TIP4P/2005 models. *The Journal of Chemical Physics*, 137(7):074503, 2012.

[27] C. G. Salzmann, P. G. Radaelli, E. Mayer, and J. L. Finney. Ice XV: A new thermodynamically stable phase of ice. *Physical Review Letters*, 103:105701, Sep 2009.

[28] P. K. Schelling, S. R. Phillpot, and P. Keblinski. Comparison of atomic-level simulation methods for computing thermal conductivity. *Physical Review B*, 65:144306, Apr 2002.

[29] G. A. Slack. Thermal conductivity of ice. *Physical Review B*, 22:3065–3071, Sep 1980.

[30] J. M. Soler, E. Artacho, J. D. Gale, A. García, J. Junquera, P. Ordejón, and D. Sánchez-Portal. The SIESTA method for ab initio order-N materials simulation. *Journal of Physics: Condensed Matter*, 14(11):2745, 2002.

[31] Y. Tajima, T. Matsuo, and H. Suga. Calorimetric study of phase transition in hexagonal ice doped with alkali hydroxides. *Journal of Physics and Chemistry of Solids*, 45(11–12):1135 – 1144, 1984.

[32] S. v. d. Walt, S. C. Colbert, and G. Varoquaux. The numpy array: A structure for efficient numerical computation. *Computing in Science & Engineering*, 13(2):22–30, 2011.

[33] B. Wehinger, D. Chernyshov, M. Krisch, S. Bulat, V. Ezhov, and A. Bosak. Diffuse scattering in Ih ice. *Journal of Physics: Condensed Matter*, 26(26):265401, 2014.

[34] M. Zhang, E. Lussetti, L. E. S. de Souza, and F. Müller-Plathe. Thermal conductivities of molecular liquids by reverse nonequilibrium molecular dynamics. *The Journal of Physical Chemistry B*, 109(31):15060–15067, 2005.

[35] X. W. Zhou, S. Aubry, R. E. Jones, A. Greenstein, and P. K. Schelling. Towards more accurate molecular dynamics calculation of thermal conductivity: Case study of GaN bulk crystals. *Physical Review B*, 79: 115201, Mar 2009.

A Appendix

A.1 Additional Parameters

In this section the additional parameters of the runs in sections 4.2 and 4.3 are listed. This includes the step that was determined as the start of the steady state, the total number of steps and the temperature difference between the hot and the cold reservoir ΔT.

A.1.1 Unordered Cells

Unordered Cells at 100K along c:			
l_z [Å]	Start [steps]	End [steps]	ΔT [K]
72.8	300 000	600 000	50
87.4	300 000	500 000	58
102.0	250 000	400 000	58
109.1	700 000	900 000	36
116.6	250 000	400 000	64
131.0	250 000	350 000	70
145.6	550 000	800 000	41
182.1	350 000	750 000	41
182.1	300 000	500 000	56
218.4	350 000	500 000	56
218.4	400 000	700 000	50
254.6	325 000	450 000	58
291.1	250 000	400 000	65
291.1	350 000	500 000	56

Table 17: The additional parameters of the simulations of unordered cells at 100K along the c direction are shown.

Unordered Cells at 150K along c:			
l_z [Å]	Start [steps]	Ending [steps]	ΔT [K]
102.0	700 000	1 000 000	50
124.1	400 000	900 000	57
145.9	500 000	800 000	68
182.3	400 000	700 000	68
219.1	400 000	700 000	78

Table 18: The additional parameters of the simulations of unordered cells at 150K along the c direction are shown.

Unordered Cells at 200K along c:			
l_z [Å]	Start [steps]	End [steps]	ΔT [K]
102.5	250 000	450 000	124
117.1	250 000	400 000	140
117.1	350 000	500 000	96
131.6	200 000	350 000	155
146.3	250 000	300 000	153
146.2	400 000	800 000	84
182.9	350 000	500 000	117
182.9	500 000	750 000	97
219.3	300 000	500 000	120
219.3	400 000	700 000	113
256.1	300 000	450 000	133
292.4	350 000	500 000	126

Table 19: The additional parameters of the simulations of unordered cells at 200K along the c direction are shown.

Unordered Cells at 100K along a/b:			
l_z [Å]	Start [steps]	End [steps]	ΔT [K]
89.5	800 000	1 000 000	27
134.2	700 000	900 000	30
178.7	500 000	800 000	39
223.5	450 000	700 000	40
268.3	400 000	600 000	42

Table 20: The additional parameters of the simulations of unordered cells at 100K along the a/b direction are shown.

A.1.2 Ordered Cells

Ordered Cells at 100K along c:			
l_z [Å]	Start [steps]	Ending [steps]	ΔT [K]
116.5	500 000	850 000	26
131.1	450 000	800 000	26
145.7	400 000	700 000	26
182.1	400 000	750 000	29
218.5	350 000	700 000	28
291.3	400 000	600 000	32

Table 21: The additional parameters of the simulations of ordered cells at 100K along the c direction are shown.

Ordered Cells at 200K along c:			
l_z [Å]	Start [steps]	Ending [steps]	ΔT [K]
117.4	450 000	750 000	53
131.8	450 000	800 000	57
146.5	450 000	800 000	61
183.1	550 000	750 000	65
256.2	450 000	650 000	79
292.5	350 000	600 000	73

Table 22: The additional parameters of the simulations of ordered cells at 200K along the c direction are shown.

Ordered Cells at 100K along a/b:			
l_z [Å]	Start [steps]	End [steps]	ΔT [K]
111.8	700 000	900 000	26
134.2	600 000	800 000	27
178.8	500 000	700 000	28
223.8	400 000	600 000	29
268.3	400 000	500 000	32

Table 23: The additional parameters of the simulations of ordered cells at 100K along the a/b direction are shown.